ACS OMEGA

Open Access



http://pubs.acs.org/journal/acsodf

Article

# Valorization and Upcycling of Acid Mine Drainage and Plastic Waste via the Preparation of Magnetic Sorbents for Adsorption of Emerging Contaminants

Bongiwe Apatia Mvala, Tshimangadzo S. Munonde, Anele Mpupa, Mokae Fanuel Bambo, Kgabo Phillemon Matabola, and Philiswa Nosizo Nomngongo*

Cite This: *ACS Omega* 2024, 9, 34700−34718

Read Online

ACCESS | Metrics & More | Article Recommendations | Supporting Information

**ABSTRACT:** Plastic waste poses a serious environmental risk, but it can be recycled to produce a variety of nanomaterials for water treatment. In this study, poly(ethylene terephthalate) (PET) waste and acid mine drainage were used in the preparation of magnetic mesoporous carbon (MMC) nanocomposites for the adsorptive removal of pharmaceuticals and personal care products (PPCPs) from water samples. The latter were then characterized using Fourier transform infrared (FTIR) spectroscopy, X-ray diffraction (XRD), scanning electron microscopy with energy-dispersive X-ray spectroscopy (SEM-EDX), transmission electron microscopy (TEM), Brunauer−Emmett−Teller (BET), and $\zeta$ potential. The results of Brunauer−Emmett−Teller isotherms revealed high specific surface areas of 404, 664, and 936 $m^2/g$ with corresponding pore sizes 2.51, 2.28, and 2.26 nm for MMC, MMAC-25%, and MMAC-50% adsorbents, respectively. Under optimized conditions, the equilibrium studies were best described by the Langmuir and Freundlich models and kinetics by the pseudo-second-order model. The maximum adsorption capacity for monolayer adsorption from the Langmuir model was 112, 102, and 106 mg/g for acetaminophen, caffeine, and carbamazepine, respectively. The composites could be reused for up to six cycles without losing their adsorption efficiency. Furthermore, prepared adsorbents were used to remove acetaminophen, caffeine, and carbamazepine from wastewater samples, and up to a 95% removal efficiency was attained.

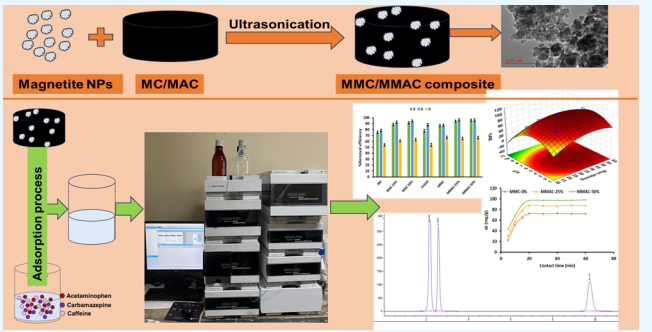


## 1. INTRODUCTION

Pharmaceuticals and personal care products (PPCPs) are generally natural or synthetic compounds used for personal care, diagnosing, preventing, or treating human or animal illnesses.[1,2] Research findings have revealed that these compounds do not completely metabolize upon consumption.[3] Instead, they are excreted both in the original and metabolized state to the sewer systems, wastewater treatment plants (WWTPs), and other aquatic/natural environments, mainly through urine and feces.[3] Subsequently, the routes to environmental contamination may also consist of effluents from industries, improper disposal by consumers, hospital effluents, and wastewater treatment plants (WWTPs).[4,5] As a result of population growth and industrialization, the use of pharmaceuticals and personal care products has increased drastically.[5] The increased use leads to their improper discharge into the environment, causing great concern as they pose a serious threat to both aquatic and terrestrial life.[6] Moreover, a number of literature reports substantiate the risks to human and animal health when these pharmaceutical and personal products are present in the environment.[7,8]

Among many concerning PPCP residues, acetaminophen (ACT), carbamazepine (CBZ), and caffeine (CAF) stand out as the most widely detected in environmental systems. Acetaminophen is one of the most commonly used over-the-counter medicines, and it is the first-line drug for the treatment of pain and fever globally.[9,10] It has been reported that about 60−70% of ACT cannot be absorbed by the human body, but it is eliminated via excretion and discharged into the sewage system.[11,12] Carbamazepine is one of the most concerning environmental pollutants. It is widely used as an anticonvulsant drug for the treatment of epilepsy, seizures, and different psychiatric disorders.[13] Due to its structural stability, persistence in nature, and difficulty in biodegrading, CBZ is one of the widely investigated emerging pollutants.[14−16]

**Received:** April 12, 2024
**Revised:** July 7, 2024
**Accepted:** July 9, 2024
**Published:** August 2, 2024

Caffeine is a psychotropic substance that is extensively used as an ingredient in pharmaceuticals, food, and beverages.[10,17] Caffeine is a substance of great pharmaceutical importance as it is responsible for physical fatigue reduction and alertness restoration. Furthermore, CAF is predominantly used as a brain, cardiac, and respiratory stimulant.[17] Similar to ACT and CBZ, CAf is frequently detected in the environmental compartment, owing to its partial removal and low degradation rate.

The presence of ACT, CBZ, and CAF in the environment is very worrying in view of the fact that they are intended to react and produce a response at low doses. Thus, they are of concern even at low concentrations.[18] Moreover, these compounds have been designed to be stable and to interact only with target molecules (proteins), which means that they are very slow to degrade in the environment.[18] Therefore, their continual usage results in a constant release and accumulation in the environment. Owing to their extensive use and consumption, acetaminophen, caffeine, and carbamazepine have been detected in concentrations ranging from ng/L to mg/L in WWTP and ground and surface waters.[19] Furthermore, it is reported that WWTPs cannot effectively treat these compounds as they are found at low concentrations.[20] Thus, it is of great importance in the scientific community to develop easy and sensitive methods of treatment that can effectively remove these compounds from various matrices.

Literature has reported several technologies that have been employed for the treatment of these micropollutants in water bodies, which include adsorption,[21,22] advanced oxidative processes,[23,24] bioremediation,[25] ion exchange,[26] and membrane separation.[27,28] Among these techniques, the adsorptive removal method has gained a lot of attention owing to its high efficiency, lower operating costs, and ease of operation and can be applied for the removal of pharmaceuticals, even in trace concentrations.[29,30] Out of many adsorbents, carbon-based adsorbents are the most broadly used for the treatment of contaminated water due to their favorable characteristics, such as their good porous structures and high surface area that confers an outstanding adsorption capacity.[31,32] Different adsorbent materials can be fabricated by making use of a wide variety of carbonaceous precursors, such as biomass waste, which can result in the production of a variety of adsorbents with different characteristics and qualities.[33] Using biomass waste has advantages that include availability and abundance, the appearance of technical effectiveness, and integration into existing processes. Despite these advantages, biomass waste has disadvantages, such as low adsorption capacity, increased chemical oxygen demand (COD), biological oxygen demand (BOD), and total organic carbon (TOC).[33]

Recently, there has been an increase in attention to the upcycling of waste materials such as PET plastic and acid mine drainage as an approach to the preparation of value-added chemicals.[34] Since plastic does not degrade, it builds up in the environment and causes serious health impacts such as choking marine wildlife, damaging soil, and poisoning groundwater.[35] On the other hand, Problems associated with mine drainage include contaminated drinking water, disrupted growth and reproduction of aquatic plants and animals, and the corroding effects of the acid on parts of infrastructures such as bridges.[36] As such, the design of adsorbents for water treatment based on plastic wastes and acid mine drainage is a promising strategy to couple plastic waste minimization with the production of new functional adsorbent materials at a low cost that can be applied to resolve pollution issues.[37] For example, carbon-based adsorbents obtained by pyrolysis of plastic waste for the adsorption of heavy metals and methylene blue dye have been designed and investigated.[38,39] Furthermore, Xinchao and colleagues successfully synthesized magnetite nanoparticles with ferric iron recovered from acid mine drainage.[40] Not long ago, Chan and Zinchenko successfully prepared a hybrid magnetic microparticle adsorbent for cesium removal by functional upcycling of waste PET plastic.[41]

Herein, we propose the synthesis of a magnetic mesoporous carbon (MMC) nanocomposite from PET waste bottles and acid mine drainage (AMD). The adsorption properties of the MMC materials were studied for the simultaneous removal of ACT, CBZ, and CAF in wastewater samples. Batch adsorption studies were carried out, and multivariate strategies were applied to investigate the effects of sample pH and dosage on the adsorbent capability. The equilibrium data for the adsorption process was analyzed in detail with adsorption isotherms, and the adsorption mechanism and rate-limiting step were evaluated using adsorption kinetics. The practical applicability and performance of the prepared adsorbents were investigated using spiked wastewater. To the best of our knowledge, there is currently no literature report of the use of MMC composites for the removal of these analytes.

## 2. EXPERIMENTAL SECTION

**2.1. Reagents and Standards.** The reagents used in this study were analytical grade, and ultrapure water (Direct-Q3UV-R purifier system Millipore, Merck, Darmstadt, Germany) was used throughout. Acetaminophen (99.9%) (ACT), caffeine (99.9%) (CAF), carbamazepine (99.9%) (CBZ), HPLC-grade methanol, acetic acid, sodium hydroxide (NaOH), ammonium hydroxide ($NH_4OH$), iron(II) chloride hexahydrate ($FeCl_2{\cdot}6H_2O$), and phosphoric acid ($H_3PO_4$) were all purchased from Sigma-Aldrich (St. Louis, MO). PET bottles were collected from waste bins at the University of Johannesburg, Doornfontein campus (Gauteng, South Africa). Acid mine drainage waste was collected from the central basin acid mine drainage treatment plant (Germiston, Gauteng, South Africa). The stock solutions were prepared by dissolving appropriate amounts of ACT, CAF, and CBZ in 100 mL of methanol. The model samples and stock solution were kept in the refrigerator at 4−8 °C, and working solutions were prepared daily by a subsequent dilution of stock solution with ultrapure water.

**2.2. Sample and Sample Collection.** Influent and effluent wastewater samples were collected from the Hammersdale (Durban, KwaZulu Natal Province, South Africa) WWTP. River water samples were collected from the Umlazi River (Durban, KwaZulu Natal Province, South Africa). Tap water samples were collected from the University of Johannesburg, Doornfontein campus (Johannesburg, Gauteng, South Africa).

**2.3. Instrumentation.** The materials were characterized using transmission electron microscopy (TEM JEOL JEM-2100, Japan), scanning electron microscopy (SEM, TESCAN VEGA 3 XMU, LMH instrument, Czech Republic) coupled with energy-dispersive X-ray spectroscopy (EDS), X-ray diffraction instrument (PANalytical BV, Almelo, Netherlands), FTIR instrument (PerkinElmer, Shelton, CT), nitrogen adsorption−desorption isotherms (Micrometrics Instrument Corp., Norcross, GA), and Nano-ZS Zetasizer (Malvern


https://doi.org/10.1021/acsomega.4c03426
ACS Omega 2024, 9, 34700−34718

**Scheme 1. Schematic Diagram Showing the Preparation of (a) Synthesis of Mesoporous Carbon (MC) and Mesoporous Activated Carbons (MACs); (b) Magnetite Nanoparticles; and (c) Magnetic Mesoporous Carbon (MMC) and Magnetic Mesoporous Activated Carbons (MMACs)**


Instruments, Malvern, UK). An inductively coupled plasma−optical emission spectrometer (ICP-OES) (iCAP 6500 Duo, Thermo Scientific, UK), a Scientech ultrasonic cleaner (Labotec, Midrand, South Africa), and an Agilent HPLC 1200 Infinity series equipped with a diode array detector (Agilent Technologies, Waldbronn, Germany) were used for leaching studies, ultrasonication, and determination of PPCPs, respectively. Detailed information about the instrumentation is provided in the Supporting Information (SI).

**2.4. Synthesis of Sorbent Materials.** *2.4.1. Preparation of Mesoporous Carbon Derived from PET Waste and Its Activation.* Mesoporous carbon (MC) was prepared from PET waste bottles using a modified method as described by Dyosiba and co-workers.[42] Scheme 1a shows a schematic diagram for the preparation of MC. The initial step involves the depolymerization of waste PET bottles that are first cut into small PET flakes, followed by their hydrolysis in a hydrothermal reactor (at 220 °C for 8 h) using a mixture of ethylene glycol and deionized water (5:95, v/v ratio), which yielded 10 g of the product. The resulting material is an organic linker called terephthalic acid (TPA), which was washed with 30 mL of ethanol three times and deionized water before being dried at 100 °C for 12 h. The product was then physically carbonated at the temperature of 725 °C in a muffle furnace for 2 h to form the mesoporous carbon.

The mesoporous carbon (2 g) was activated by dispersing it in 25 mL of 25 and 50% KOH solution (6.25 g in 25 mL and 12.5 g in 25 mL, Figure 1a). The solution was then heated at 100 °C for 12 h, and the resulting sludge was transferred into a crucible. This was followed by physical activation at 700 °C in a muffle furnace for 2 h. The product was then washed with warm water and 10 mL of 1% of HCl. After the product was washed three times with water, the sample attained a neutral pH (∼7). The final product was then dried at 100 °C and kept there until use.

*2.4.2. Preparation of Magnetite Nanoparticles.* The synthesis of magnetite was done following the method described in the literature[43] with slight modifications (Scheme 1b). Briefly, 500 mL of acid mine drainage (AMD) was transferred into an 800 mL beaker, and the pH was increased from 2.7 to approximately 4.5 by gradually adding drops of a 10% NaOH solution to precipitate the Fe(III) completely. The Fe(III) precipitate was then separated by means of centrifugation. After that, the Fe(III) sludge was stored in a refrigerator at 4 °C until further use.

Commercial $FeCl_2{\cdot}6H_2O$ was used as the source of Fe(II). Briefly, 4 g of Fe(III) wet sludge was dissolved in enough ultrapure water (100−150 mL) in a 250 mL round-bottom flask and stirred at 80 °C. Then, 2 g of $FeCl_2.6H_2O$ was transferred into the solution while continuously stirring. The reaction was performed under an $N_2$(g) atmosphere to remove the dissolved oxygen from the solution completely. Then, 20 mL of a 28% $NH_4OH$ solution was transferred into the reaction, and the solution immediately turned black. The reaction was left to stir vigorously for 30 min to precipitate the magnetite completely. The black precipitate (magnetite) was then separated from the solution by an external magnet and washed with deionized water until the neutral pH (∼7.5) and then vacuum-dried.

*2.4.3. Preparation of Magnetic Mesoporous Carbon (MMC) or Magnetic Mesoporous Activated Carbons (MMAC).* The MMC or MMAC adsorbents were synthesized via an ultrasonication method (Scheme 1c). First, 1 g of synthesized pristine MC or MAC was placed into a clean beaker, followed by the addition of 100 mL of ethylene glycol as an adhesion/binding agent.[44] The solution was then sonicated for 1 h to disperse the carbon in the solution properly. Then, 1 g of magnetite was added to the aforementioned solution and further sonicated for another 1 h. The product was separated via centrifugation, washed


https://doi.org/10.1021/acsomega.4c03426
ACS Omega 2024, 9, 34700−34718

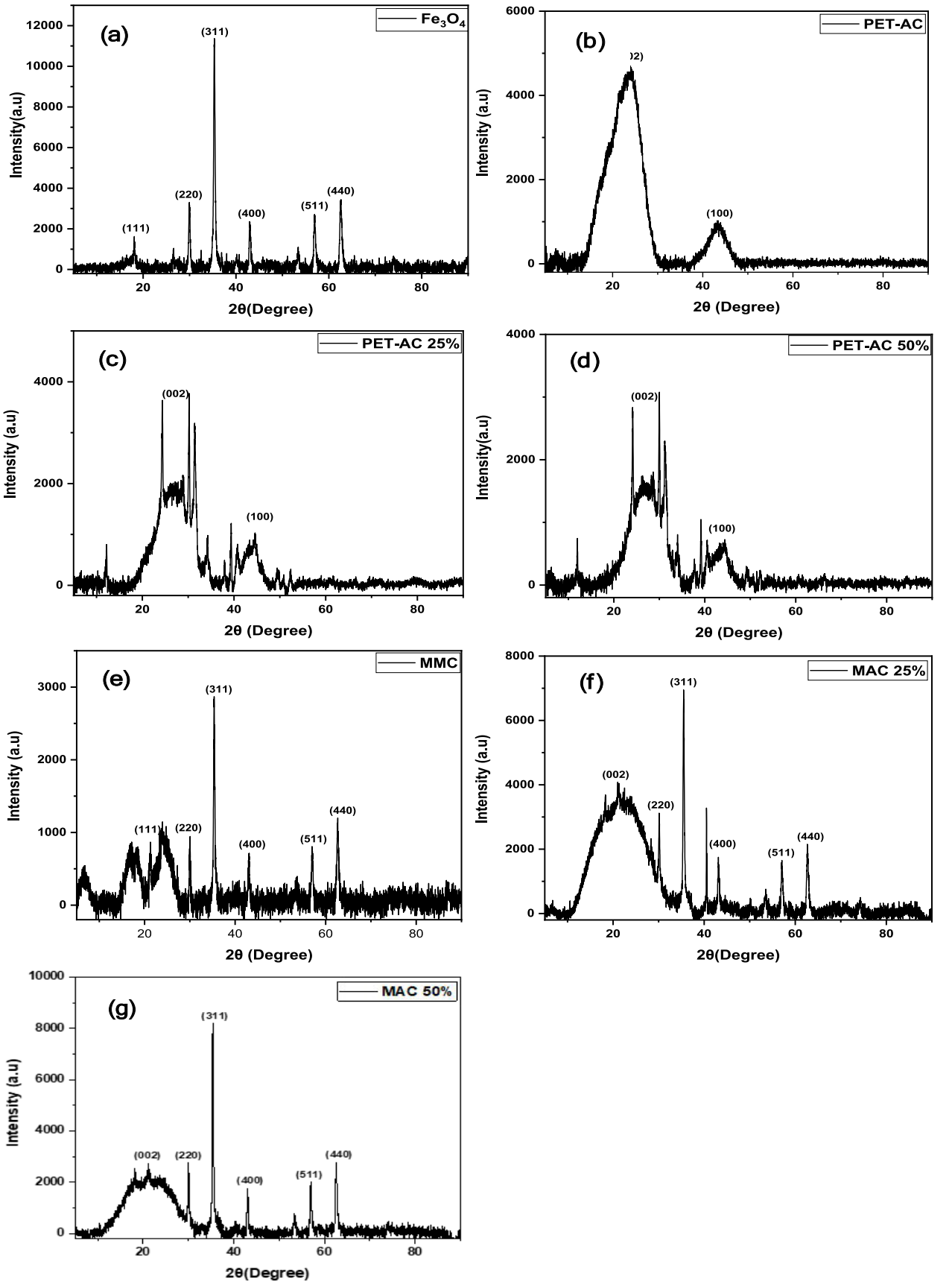


**Figure 1.** XRD patterns of (a) mesoporous carbon (MC), (b) mesoporous activated carbon (MAC-25%), (c) MAC-50%, (d) $Fe_3O_4$, (e) magnetic mesoporous carbon (MMC), (e) magnetic mesoporous activated carbon (MMAC-25%), (f) magnetic mesoporous activated carbon (MMAC-25%), and (g) MMAC-50%.



https://doi.org/10.1021/acsomega.4c03426
ACS Omega 2024, 9, 34700−34718

several times with deionized water, and then dried for 8 h at 100 °C.

**2.5. Batch Adsorption Experiments.** The adsorption study was employed by the batch adsorption method. In the experiments, appropriate amounts (56.2 mg) of the adsorbents were weighed and placed into clean glass bottles, followed by 10 mL aliquots of the synthetic sample containing the mixture of analytes (ACT, CAF, and CBZ) at concentrations of 1.0 mg/L adjusted at different pH values (3−9). The sample solutions were then agitated in an ultrasound water bath for 30 min, and thereafter, the adsorbent(s) were separated from the supernatant by an external magnet. After separation, 1 mL of the supernatant was filtered by a 0.22 $\mu$m PVDF filter and then analyzed using the HPLC-DAD. The filtration step was conducted to remove any foreign fine particles that might be in the sample as well as to avoid blockage of the injection port and tubing. The adsorption removal efficiency (%RE) was calculated by eq 1

$$\%\mathrm{RE} = \frac{C_0 - C_e}{C_0} \times 100 \quad (1)$$

where $C_0$ and $C_e$ are the initial and equilibrium concentrations, respectively.

A central composite design (CCD) method was employed to optimize the influential variables (mass of adsorbent and pH) for the adsorption of ACT, CAF, and CBZ on the surfaces of the adsorbents. Under optimum conditions, the equilibrium isotherms, kinetics, and thermodynamics were investigated. The equilibrium isotherms were conducted by varying the sample concentrations in the range of 5−50 mg/L with a sample volume of 10 mL and 30 min sonication time. The isotherm studies were performed in triplicate, and the adsorption capacity ($q_e$, mg/g) was calculated by eq 2

$$q_e = \frac{(C_0 - C_e)V}{C_0} \quad (2)$$

where $C_0$ and $C_e$ are the initial and equilibrium concentrations (mg/L), respectively, m is the mass (g) of the adsorbent, and $V$ is the volume (L) of the sample solution. The adsorption kinetics were studied by varying contact time from 5−60 min for each sample before analysis. The kinetics experiments were conducted using initial concentrations of 50 mg/L, sample pH of 7, and adsorbent mass of 56.2 mg. The concentration of analytes in aqueous solution was determined using HPLC-DAD. The adsorption capacity ($q_t$) at time, t, was calculated using eq 3.

$$q_t = \frac{(C_0 - C_t)V}{C_0} \quad (3)$$

where $q_t$ and $C_t$ are the adsorption capacity (mg/g) and concentrations (mg/L) of the analytes at time $t$. The impact of temperature on the adsorption capacities of the adsorbents toward ACT, CAF, and CBZ was investigated by performing the adsorption process at varying temperatures (25−45 °C). During this process, the mass of the adsorbent, pH, contact time, sample volume, and initial concentrations were all fixed.

**2.6. Regeneration and Reusability Studies.** To explore the reusability of the prepared adsorbents, 56.2 mg of each adsorbent was placed into a glass bottle, and 10 mL of sample solution containing 50 mg/L was added to the bottle, followed by ultrasonication for 30 min. After that, the adsorbent was separated from the supernatant with an external magnet. Preliminary results have proved that a minimum of 2 mL of methanol was suitable for complete desorption of the analytes from the surface of the adsorbent. Therefore, the resultant adsorbent was washed with 2 mL of methanol three times to remove the adsorbed analytes. Then, 1.0 mL of the composite methanol phase (all methanol extraction fractions were combined) containing the analytes of interest was separated using an external magnet and analyzed with HPLC-DAD. The adsorbent was then washed with a 10 mL mixture of ultrapure water and ethanol, followed by rinsing three times with 5 mL of ethanol. The spent adsorbent was dried in the oven at 60 °C for 2 h before reuse. The adsorption−desorption process was repeated five times. Furthermore, the stability of the adsorbents was evaluated by determining the iron concentrations in the supernatant solutions after every cycle using inductively coupled plasma optical emission spectrometry (ICP-OES).

**2.7. Real Water Sample Analysis and Method Validation.** As a proof of concept, the adsorption process was applied to remove selected PPCPs from water samples. The WWTP influent, WWTP effluent, and surface water samples were collected from Hammarsdale WWTP. The tap water samples were collected from the laboratory. All samples were first analyzed for their physicochemical characteristics, namely, pH, electrical conductivity (EC), total dissolved solids (TDS), turbidity, and chemical oxygen demand (COD). The results are presented in Table S1 (Supporting Information). A solid phase extraction method employing HLB as a sorbent material coupled with HPLC-DAD was used to characterize the water samples, and the results are presented in Table S1. The results obtained showed that the target analytes were detected in wastewater samples and surface water samples. Therefore, to test the effectiveness of the prepared adsorbents, the samples were spiked at levels (0.1 and 2.0 mg/L) representing the relevant concentrations of wastewater (influents and effluents) and surface water samples. The optimized adsorption process was applied to remove ACT, CAF, and CBZ.

## 3. RESULTS AND DISCUSSION

**3.1. Fourier Transform Infrared (FTIR) Spectroscopy.** Figure S1 shows the FTIR spectra of the as-synthesized (a) (MC), (b) MAC-25%, (c) MAC-50%, (d) $Fe_3O_4$, (e) MMC, (g) MMAC-25%, and (g) MMAC-50%. All of the spectra displayed a broad band at 3410 and 2000 $cm^{-1}$, which were ascribed to the OH stretching vibration of the absorbed water and O═C═O, which is the atmospheric $CO_2$ absorbed from moisture. The bands at 2981, 1384, and 813 $cm^{-1}$ were assigned to the $CH_2$ and $CH_3$ stretching and bending vibrations on the mesoporous carbons, including the nanocomposites. The bands found at wavenumbers 1628 and 1139 $cm^{-1}$ were attributed to the C═O and C−O vibrations of the carbonyl groups, and the 949 $cm^{-1}$ was ascribed to the C═C stretching, which agrees with the FTIR spectrum of the carbon material reported in the literature.[6] All of the compounds comprising the mesoporous carbon displayed all of these characteristics. The bending peaks at 590 and 503 $cm^{-1}$ were reported to represent the characteristic vibrations of Fe−O corresponding to the magnetite nanoparticles.[45]

**3.2. X-ray Diffraction (XRD) Spectroscopy.** The crystal structure was studied, and the XRD patterns of the (a) mesoporous carbon (MC), (b) mesoporous activated carbon (MAC-25%), (c) MAC-50%, (d) $Fe_3O_4$, (e) magnetic


https://doi.org/10.1021/acsomega.4c03426
ACS Omega 2024, 9, 34700−34718

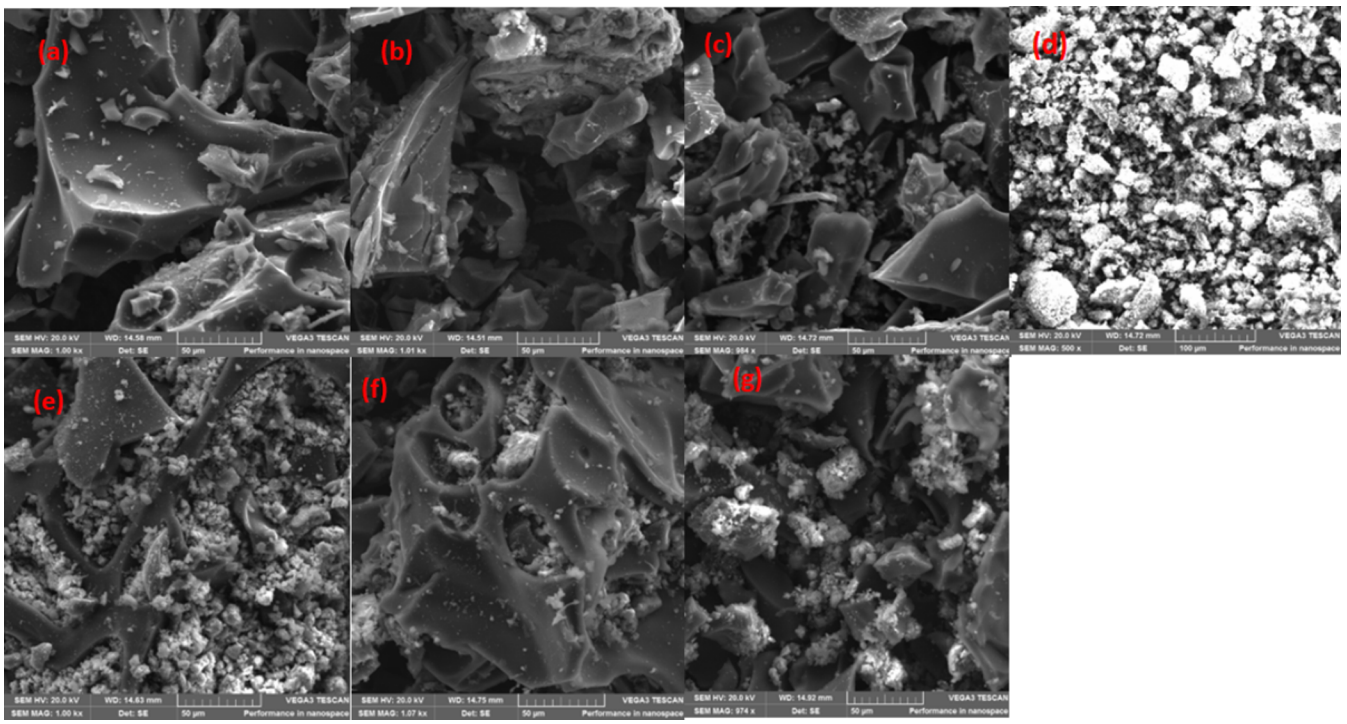


**Figure 2.** SEM of (a) mesoporous carbon (MC), (b) mesoporous activated carbon (MAC-25%), (c) MAC-50%, (d) $Fe_3O_4$, (e) magnetic mesoporous carbon (MMC), (f) magnetic mesoporous activated carbon (MMAC-25%), and (g) MMAC-50%.

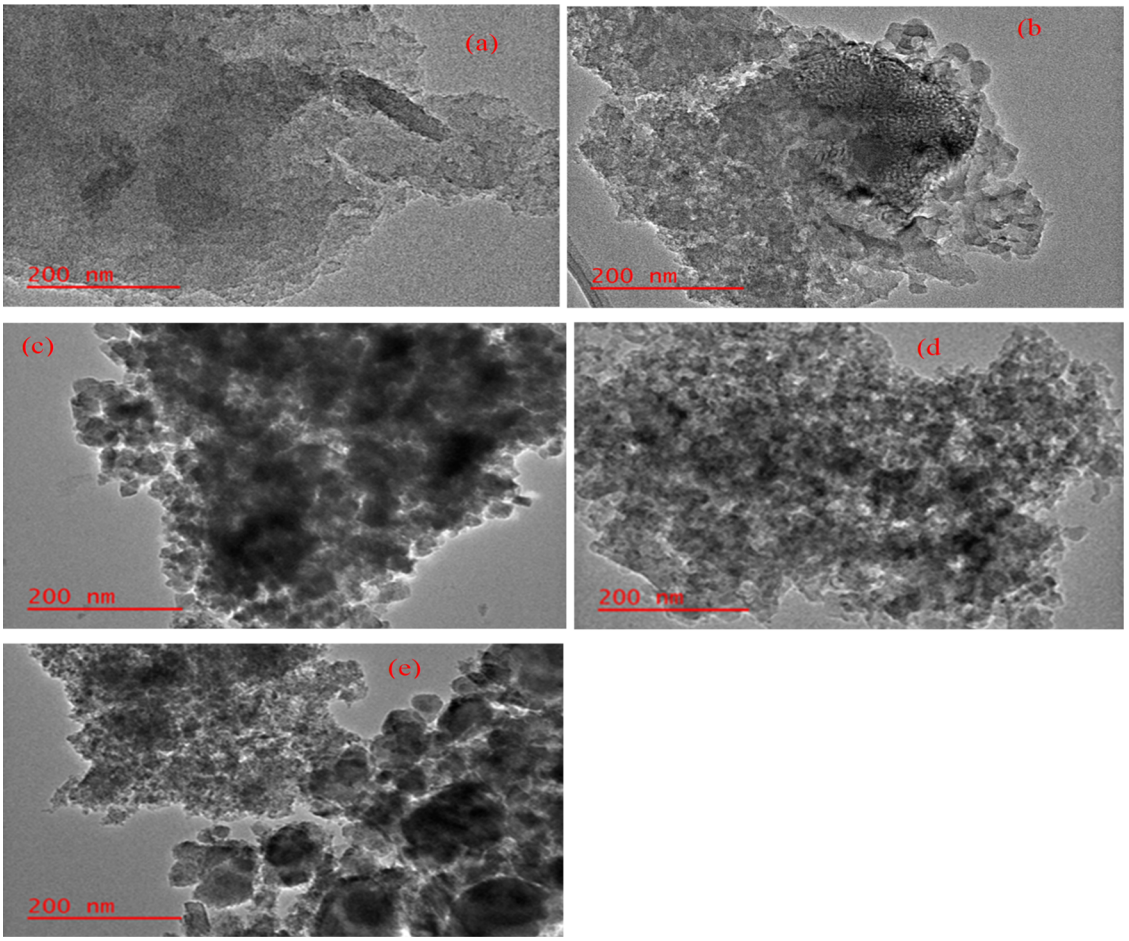


**Figure 3.** TEM images (a) mesoporous carbon, (b) mesoporous activated carbons, (c) $Fe_3O_4$, (d) magnetic mesoporous carbon (MMC), and (e) magnetic mesoporous activated carbons (MMAC).



https://doi.org/10.1021/acsomega.4c03426
*ACS Omega* 2024, 9, 34700−34718

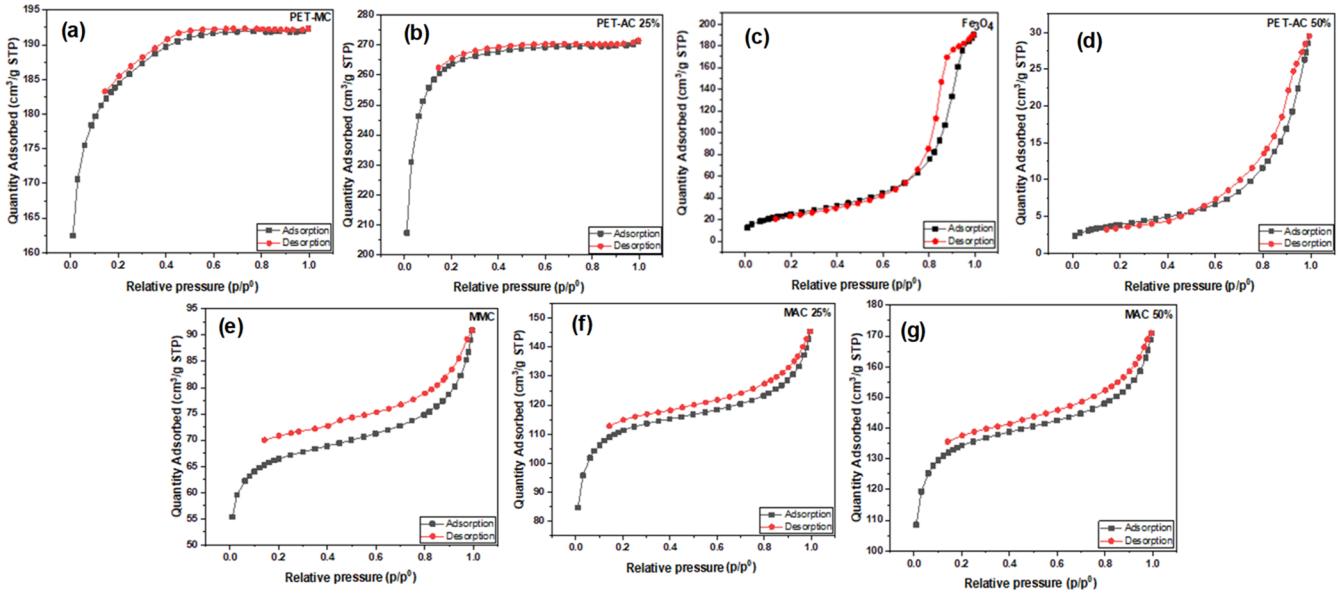


**Figure 4.** $N_2$ adsorption and desorption isotherms at 77 K (a) mesoporous carbon (MC), (b) mesoporous activated carbon (MAC-25%), (c) $Fe_3O_4$, (d) mesoporous activated carbon (MAC-50%), (e) magnetic mesoporous carbon (MMC), (f) magnetic mesoporous activated carbon (MMAC-25%), and (g) magnetic mesoporous activated (MMAC-50%).

mesoporous carbon (MMC), (f) magnetic mesoporous activated carbon (MMAC-25%), and (g) MMAC-50% are shown in Figure 1. The XRD pattern revealed the good orientation and purely crystalline nature of the iron oxide nanoparticles. It was found to be comparable to the carbon and the magnetite reported in the literature.[46] The diffraction peaks at $2\theta$ = 19.5, 30.0, 35.4, 43.0, 57.0, and 62.6° were indexed and ascribed to the (111), (220), (311), (400), (511), and (440) magnetite planes, and the sharp peaks displayed the crystalline nature of magnetite.[46] The XRD patterns of magnetite powder synthesized with ferric iron recovered from AMD were almost identical with that of the sample prepared with reagent-grade chemicals, indicating that the purity of the resolubilized ($Fe_2(SO_4)_3$) solution recovered from AMD was sufficient for magnetite synthesis. The XRD patterns of the carbon materials displayed two broad peaks, which revealed the amorphous nature of carbon. The diffraction peaks at $2\theta$ = 24.1 and 43.3° correspond to the carbon planes indexed to (002) and (100), respectively, in the compounds containing carbon. The MAC-25% and MAC-50% sharp peaks depict small amounts of KOH that were used in the activation phase. The MMAC, MMAC-25%, and MMAC-50% displayed both the properties of carbon and magnetite nanoparticles, which confirmed the impartation of the magnetite nanoparticles onto the carbon.

**3.3. Scanning Electron Microscopy/Energy-Dispersive X-ray Spectroscopy (SEM/EDX).** Morphological properties are important in determining the homogeneity or heterogeneity of the materials. This indicates the uniformity of the material. SEM was used to investigate the surface morphology of the synthesized materials, and their micrographs are presented in Figure 2 (a) MC, (b) MAC-25%, (c) MAC-50%, (d) $Fe_3O_4$, (e) MMC, (f) MMAC-25%, and (g) MMAC-50%. Figure 2a–c shows sheet-like structures of mesoporous carbon stacked on top of one another. The SEM image in Figure 2d reveals a spherical structure of the magnetite nanoparticles of varying sizes, which are aggregated because of magnetic field properties. Similar results have been reported in the literature.[47] The nanocomposite images in Figure 2e,f clearly showed the magnetite nanoparticles embedded in the pores and the surface of the carbon sheets. This confirms the successful incorporation of nanoparticles within mesoporous carbon.

The EDX spectrum of the magnetite nanoparticles showed that the material was dominated by Fe and O atoms with elemental composition of 72.5 and 20.4%, respectively, with oxygen confirming the formation of magnetite, while the presence of 4.1% of Cl was from the $FeCl_2{\cdot}4H_2O$ reagent (Figure S2a). The presence of traces of Al, Mg, Mn, and Si indicated that there was coprecipitation of these elements during the recovery of Fe (III) species from AMD. The EDX studies of the nanocomposites also revealed the elemental compositions, which are represented by carbon (C), iron (Fe), oxygen(O), sulfur (S), and potassium (K) resulting from AMD.

**3.4. Transmission Electron Microscopy.** The TEM images from Figure 3a,b show flat sheets of mesoporous carbon with visible pores in both the MC and MAC materials. Figure 3c reveals the shape of the synthesized nanoparticles, which ranged from cubic to spheroidal, which was consistent with the literature.[47] The particle size and morphology were almost identical with the ones synthesized from commercial chemicals. Therefore, ferric iron recovered from AMD proved to be a low-cost feedstock substitute for commercial ferric salts for the synthesis of magnetite nanoparticles. The TEM images in Figure 3e–g showed the incorporation of the magnetite nanoparticles on the carbon materials. The nanoparticles were found to be uniformly dispersed on the carbon sheets.

**3.5. Nitrogen Adsorption–Desorption.** Textural properties of an adsorbent are very important, as they influence the adsorption efficiency, especially in complex matrices (such as wastewater). The specific surface area and porosity have been reported to be highly associated with the maximal adsorption capacity of the adsorbent.[48,49] BET was employed to examine the structural properties of the synthesized compounds. The $N_2$ adsorption–desorption isotherms in Figure 4 describe the type and porosity of the material. Figure 4a,b shows type 1


https://doi.org/10.1021/acsomega.4c03426
ACS Omega 2024, 9, 34700–34718

isotherm graphs with no hysteresis loop for mesoporous carbon and MAC-50%.

Meanwhile, magnetite, MMC, MAC-25%, and MAC-50% showed type IV isotherm graphs with a hysteresis loop, which is mainly characterized by monolayer adsorption. The uptake continuously increases with pressure and reaches a plateau at the saturation pressure. The pore size distribution graphs (Figure S3) confirmed the mesoporous nature of the materials, as the distribution is mostly in the mesoporous range. Table 1 gives a summary of the surface properties of the synthesized materials. The specific surface area for magnetite, mesoporous carbon MAC-25%, and MAC-50% were found to be 90.8, 563, and 853, and 1037 $m^2/g$, the average pore size of 12.7, 2.11, 1.96, and 2.13 nm, along with the pore volume 0.27, 0.30, 0.42, and 0.35 $cm^3/g$ respectively. While the MMC, MAC-25%, and MAC-50% gave a specific surface area of 404, 664, and 936 $m^2/g$ with corresponding pore size of 2.51, 2.28, and 2.26 nm and pore volume of 0.13, 0.21, and 0.25 $cm^3/g$ respectively. Activating the carbon increased the pore volume, and depositing magnetite reduced the pore volume; however, the pore size was not greatly affected. The resulting decrease in the specific surface area of the nanocomposite verified the deposition of magnetite nanoparticles on the surface of the carbon materials.

**Table 1. Surface Properties of Magnetite, Mesoporous Carbon, MAC-25%, MAC-50%, Magnetic Mesoporous Carbon, MMAC-25%, and MMAC-50%**

| material | surface area ($m^2/g$) | pore volume ($cm^3/g$) | pore size (nm) |
|---|---|---|---|
| magnetite | 90.8 | 0.27 | 12.7 |
| mesoporous carbon | 563 | 0.30 | 2.11 |
| MAC-25% | 853 | 0.42 | 1.96 |
| MAC-50% | 1037 | 0.35 | 2.13 |
| magnetic mesoporous carbon | 404 | 0.13 | 2.51 |
| MMAC-25% | 664 | 0.21 | 2.28 |
| MMAC-50% | 936 | 0.25 | 2.26 |

**3.6. Adsorption Studies of Acetaminophen, Caffeine, and Carbamazepine onto Adsorbents.** *3.6.1. Choice of Adsorbents.* The capacities of MC, MAC-25%, MAC-50%, $Fe_3O_4$, MMC, MMAC-25%, and MMAC-50% adsorbents for the adsorption of ACT, CAF, and CBZ were investigated as a function of pH, and the results are illustrated in Figure S4. As seen, the removal efficiencies of each adsorbent material toward ACT, CAF, and CBZ significantly changed as the pH of the solution changed. This phenomenon suggests that sample pH may have changed the adsorbents' surface activity properties and physiochemical features of the analytes. Figure 7 shows that all of the investigated adsorbents showed quantitative removal efficiencies toward ACT, CAF, and CBZ between pH 4 and 6. The effect of pH on the adsorption of the target analytes will be discussed in detail at a later stage. The typical trend was that the mesoporous activated carbons and composites had slightly better adsorption performance compared to MC and magnetite. In addition, these findings were coherent with the results of $N_2$-adsorption−desorption, suggesting that there was a compelling proportional correlation between the surface properties of the adsorbent and their removal efficiencies. Although all of the investigated materials proved to be suitable for the adsorptive removal of ACT, CAF, and CBZ, magnetic materials (excluding magnetite) were chosen for further studies. This is because magnetite facilitated the ease of separation and recovery of the adsorbent from the aqueous solutions. In addition, the results have proven that the combination of carbon materials and magnetic nanoparticles has intensified the adsorption efficiency of the resultant adsorbent in the order MMAC-50% > MMAC-25% > MAC.

*3.6.2. Optimization of the Experimental Parameters.* The batch adsorption studies were optimized using a central composite design (CCD), and the design matrix with the obtained respective responses (%removal efficiency, %RE) at the corresponding experimental conditions is illustrated in Table S2. Statistica software was used to interpret and explain the adsorption data in Table S2. A Pareto chart based on the analysis of variance (ANOVA) was used to analyze the effects of influential parameters by evaluating the variance within the experimental design matrix (Figure S5). As shown in Figure S5A, the sample and dosage were significant at the 95% confidence level because the bar length exceeded the reference red line ($p = 0.05$), while in Figure S5B, only the sample pH was statistically important. The 3D response surface plots were used to visualize the interactions between dosage and sample

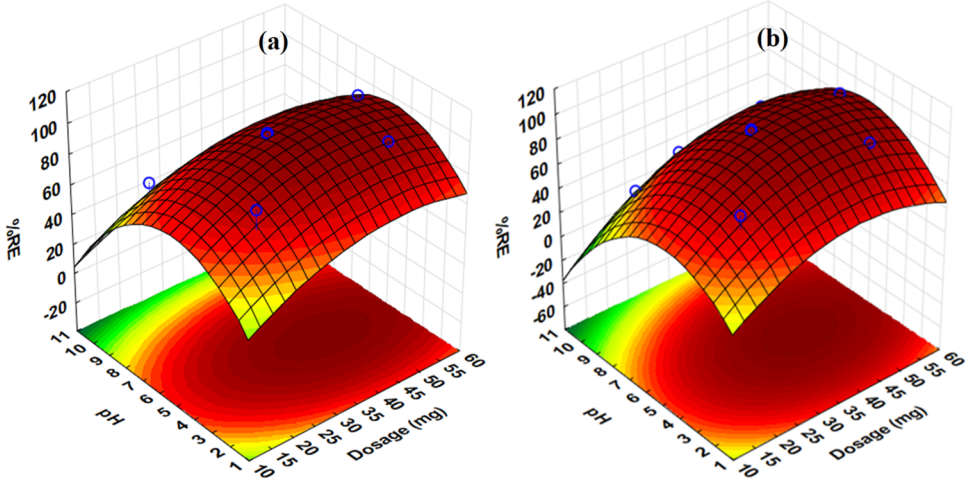


**Figure 5.** 3D plots for the interaction of optimum parameters for the adsorptive removal of acetaminophen using (a) magnetic mesoporous carbon and (b) magnetic mesoporous activated carbons.



https://doi.org/10.1021/acsomega.4c03426
ACS Omega 2024, 9, 34700−34718

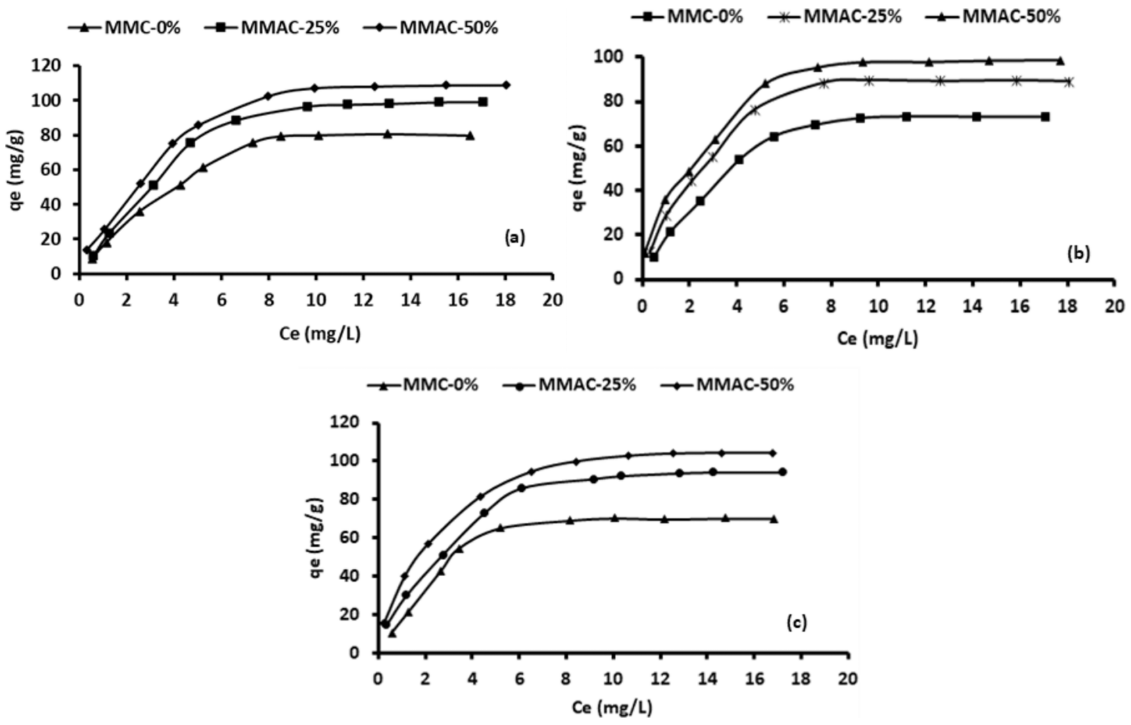


**Figure 6.** Effect of (a) ACT, (b) CAF, and (c) CBZ concentration (mg/L) on adsorption capacity qe (mg/g) of MMC-0%, MAC-25%, and MAC-50% adsorbents. Experimental conditions: contact time: 30 min; mass of absorbent: 56.2 mg; pH: 7; room temperature; sample volume: 10 mL.

**Table 2. Nonlinear Adjusted Adsorption Isotherms and Parameters Investigated**[a]

| Models | Parameters | MMC | | | MMAC-25% | | | MMAC-50% | | |
|---|---|---|---|---|---|---|---|---|---|---|
| | | ACT | CAF | CBZ | ACT | CAF | CBZ | ACT | CAF | CBZ |
| | $q_{exp}$ (mg/g) | 80.5 | 73.2 | 70.2 | 99.1 | 88.9 | 94.3 | 109 | 98.7 | 104 |
| **Langmuir** | $q_{max}$ (mg/g) | 81.7 | 76.3 | 73.5 | 102 | 94.5 | 98.7 | 112 | 102 | 106 |
| | $K_L$ (L/mg) | 0.21 | 0.31 | 0.38 | 0.24 | 0.39 | 0.35 | 0.29 | 0.43 | 0.46 |
| | Adjusted $R^2$ | 0.9944 | 0.9927 | 0.9949 | 0.9971 | 0.9966 | 0.9937 | 0.9976 | 0.9988 | 0.9946 |
| | RSE | 1.25 | 1.27 | 1.03 | 1.17 | 1.08 | 1.02 | 1.15 | 1.06 | 1.18 |
| | $\chi^2$ | 0.89 | 0.38 | 0.87 | 0.29 | 0.59 | 0.76 | 0.12 | 0.63 | 0.63 |
| **Freundlich** | $K_F$ [(mg/g)(L/mg)$^{1/n}$] | 25.6 | 27.5 | 29.1 | 32.1 | 31.7 | 37.1 | 39.4 | 35.4 | 44.7 |
| | N | 1.53 | 2.35 | 2.13 | 2.28 | 2.21 | 2.17 | 2.5 | 2.03 | 2.20 |
| | Adjusted $R^2$ | 0.9945 | 0.9939 | 0.9913 | 0.9946 | 0.9942 | 0.9915 | 0.9953 | 0.9957 | 0.9908 |
| | RSE | 1.49 | 1.32 | 1.37 | 1.33 | 1.36 | 1.15 | 1.26 | 1.13 | 1.26 |
| | $\chi^2$ | 1.02 | 0.53 | 1.03 | 0.29 | 0.55 | 0.83 | 0.25 | 0.74 | 0.77 |
| **D–R** | $q_{D-R}$ (mg/g) | 75.4 | 70.8 | 66.4 | 86.5 | 79.7 | 84.7 | 86.5 | 86.3 | 95.3 |
| | β (mol$^2$/kJ$^2$) | 0.0017 | 0.0013 | 0.0016 | 0.00055 | 0.00037 | 0.00048 | 0.00042 | 0.00034 | 0.00035 |
| | $E_a$ (kJ/mol) | 17.1 | 19.6 | 17.7 | 30.2 | 36.8 | 32.3 | 34.5 | 38.3 | 37.8 |
| | Adjusted $R^2$ | 0.9765 | 0.9817 | 0.9788 | 0.9785 | 0.9837 | 0.9865 | 0.9877 | 0.9836 | 0.9887 |
| | RSE | 5.48 | 3.54 | 3.53 | 3.47 | 2.87 | 2.14 | 2.94 | 1.73 | 1.47 |
| | $\chi^2$ | 6.17 | 2.19 | 2.66 | 1.91 | 1.93 | 1.75 | 1.54 | 1.51 | 1.11 |

[a] $q_e$ (mg/g): amount adsorbed; qmax (mg/g): maximum monolayer adsorption; $K_L$ (L/mg): Langmuir constant; $C_e$ (mg/L); concentration of adsorbate at equilibrium; $R_L$: separation factor; $K_F$ (L/mg): adsorption capacity; $1/n$: adsorption intensity; Dubin constant: $E$ (kJ/mol): mean adsorption energy: Polanyi potential; $R$: gas constant; $T$: temperature.

pH (Figure 5). As seen, the removal efficiency increased with increasing dosage. This could be attributed to increased active sites available for adsorption of the analyte.

To understand the effect of pH on the adsorption, the point of zero charge of the adsorbents (MMC, MMAC-25%, and MMAC-50%) was considered. As shown in Figure 5, the adsorption of the analyte increased with increasing sample pH up to 6. This pH value is lower than the point of zero charges of MMC, which is 8.01 and higher than those for MMAC-25% and MMAC-50% (4.9) (Figure S6). This suggests that the surface of the material was positively charged for MMC and negative for MMAC-25% and MMAC-50%. The analytes had p$K_a$ values of 9.51, 14.0, and 13.9 for ACT, CAF, and CBZ, meaning that at this pH range, the analytes are in their


https://doi.org/10.1021/acsomega.4c03426
ACS Omega 2024, 9, 34700−34718

Table 3. Nonlinear Adjusted Adsorption Isotherms and Parameters Investigated[a]

| Models | Parameters | MMC | | | MMAC-25% | | | MMAC-50% | | |
|---|---|---|---|---|---|---|---|---|---|---|
| | | ACT | CAF | CBZ | ACT | CAF | CBZ | ACT | CAF | CBZ |
| | $q_{exp}$ (mg/g) | 80.5 | 73.2 | 70.2 | 99.1 | 88.9 | 94.3 | 109 | 98.7 | 104 |
| R-P | $K_{R\text{-}P}$(L/g) | 15.5 | 17.1 | 14.3 | 13.6 | 14.5 | 13.4 | 12.4 | 13.6 | 12.4 |
| | $\sigma_{R\text{-}P}$(L/mg) | 0.87 | 0.94 | 0.94 | 0.89 | 0.98 | 1.08 | 0.77 | 0.96 | 0.87 |
| | B | 0.85 | 0.90 | 0.85 | 0.84 | 0.95 | 0.87 | 0.71 | 0.91 | 0.76 |
| | $R^2$ | 0.9945 | 0.9958 | 0.9955 | 0.9989 | 0.9957 | 0.9936 | 0.9977 | 0.9945 | 0.9943 |
| | RSE | 1.13 | 1.09 | 1.26 | 1.04 | 1.05 | 1.85 | 1.07 | 1.04 | 1.05 |
| | □$^2$ | 0.88 | 0.65 | 0.88 | 0.78 | 0.36 | 1.46 | 0.69 | 0.49 | 0.78 |
| Sips | $q_{ms}$(mg/g) | 82.3 | 76.5 | 73.1 | 104 | 96.7 | 102 | 113 | 106 | 107 |
| | $K_S$(L/mg) | 0.11 | 0.26 | 0.27 | 0.28 | 0.37 | 0.34 | 0.054 | 0.42 | 0.46 |
| | $n_S$ | 1.23 | 1.48 | 1.85 | 1.19 | 1.29 | 1.21 | 1.07 | 1.11 | 1.02 |
| | $R^2$ | 0.9966 | 0.9936 | 0.9985 | 0.9991 | 0.9966 | 0.9982 | 0.9989 | 0.9984 | 0.9976 |
| | RSE | 1.16 | 1.05 | 1.03 | 1.07 | 1.04 | 1.13 | 1.05 | 0.94 | 1.03 |
| | □$^2$ | 0.55 | 0.11 | 0.19 | 0.23 | 0.16 | 0.73 | 0.18 | 0.22 | 0.55 |

[a]$K_R$ (L/g) and $\sigma_R$ (L/mg): Redlich−Peterson constants; B: slope; $q_{mS}$ (mg/g): Sips maximum adsorption capacity; $K_S$ (L/mg): Sips isotherm model constant; $n_S$: Sips isotherm model exponent.

molecular state.[50−52] This translates to the presence of the lone pairs on the analytes to be available for ionic interaction with the positively charged MMC. For the MMAC-25% and MMAC-50%, the mechanism of adsorption is suggested to include pore filling and $\pi-\pi$ interactions.[53]

The optimal experimental conditions for the investigated factors were estimated by applying the desirability function. Desirability score ranging from 0−1 (where 0, 0.5, and 1 correspond to the least desired, middle, and most desirable response). According to Figure S7, the optimum experimental conditions for the adsorption of selected PPCPs were 6 and 56 mg for sample pH and MA. The predicted optimum conditions were validated and confirmed experimentally (six replicates). The experimental and predicted responses are presented in Table S4. According to the Student t-test (paired two samples for means), the results were not significantly different at a 95% confidence level. This is because the $t_{calculated}/t_{stat}$ was less than $t_{critical}$.

**3.7. Equilibrium Studies.** Isotherm models are used to describe the interaction between the analyte and the adsorbent at dynamic equilibrium after a certain incubation time.[54] Furthermore, the isotherm models demonstrate the economic feasibility of the adsorbent for viable applications, thus influencing the adsorption experimental design for an industrial-scale process.[55] In this instance, the isotherms for ACT, CAF, and CBZ were used to explain the sorption mechanism on the surface of the adsorbents (MMC, MMAC-25%, and MMAC-50%). It was observed that the adsorption capacity increased with increasing analyte concentration until it reached equilibrium (Figure 6). This increase in adsorption capacity was attributed to higher initial analyte (ACT, CAF, and CBZ) concentrations, which created a greater driving force by hastening the diffusion of the adsorbate molecules onto the surface of the adsorbent.[56] The equilibrium adsorption data was fitted into five nonlinear isotherm models, including the Langmuir, Freundlich, Dubin−Radushkevich, Redlich−Peterson, and Sips. Various studies have applied the linear regression of adsorption models for the estimation of isotherm parameters (Batool et al., Hamzaoui and Bestani, Okpara et al.).[57−5859] However, previous studies have reported that linearizing the models is not suitable for the estimation of isotherm parameters, thus leading to erroneous conclusions.[60,61]

Furthermore, researchers have recommended the use of coefficient of determination ($R^2$) to decide on the best-fitting isotherm models, which was found to be misleading and insufficient.[62,63] Therefore, nonlinear regression models were used to estimate the isotherm parameters. The values of the nonlinear regression model parameter for ACT, CAF, and CBZ adsorption by MMC-0%, MMAC-25%, and MMAC-50% are presented in Tables 2 and 3.

*3.7.1. Two-Parameter Isotherm Models.* The data in Figure 6 was fitted into two-parameter nonlinear models, including Langmuir, Freundlich, and Dubin−Radushkevich isotherms. The isotherm parameter values calculated from the nonlinear expressions of these models are summarized in Table 2. The nonlinear isotherm regression analysis revealed that the ACT, CAF, and CBZ data were better described by the Langmuir and Freundlich models (Table 2) than the Dubin−Radushkevich model. This is supported by the higher correlation of the determination and lower RSE and $\chi^2$ values. These findings suggest that the adsorption behavior of ACT, CAF, and CBZ onto magnetic carbon-based adsorbents could not be explained by one isotherm model but by the combination of the two models.[64] These results suggest that the adsorption process was monolayer adsorption on a heterogeneous adsorbent surface.[65,66] The results show that maximum adsorption capacity and Langmuir affinity constants ($K_L$) for all of the analytes followed the trend: MMC-0% > MMAC-25% > MMAC-50%. This might be related to the increased oxygenated functional groups introduced during the activation of the mesoporous carbon. Furthermore, the BET surface area of the synthesized carbon-based adsorbents proved to play a critical role in their adsorption behavior (Table 1). Moreover, the values of the $K_L$ were low, confirming the high affinity between the analyte molecules and the adsorbents' active sites.[64] The separation factor ($R_L$) estimated from the Langmuir model parameters was used to assess the adsorption


https://doi.org/10.1021/acsomega.4c03426
ACS Omega 2024, 9, 34700−34718

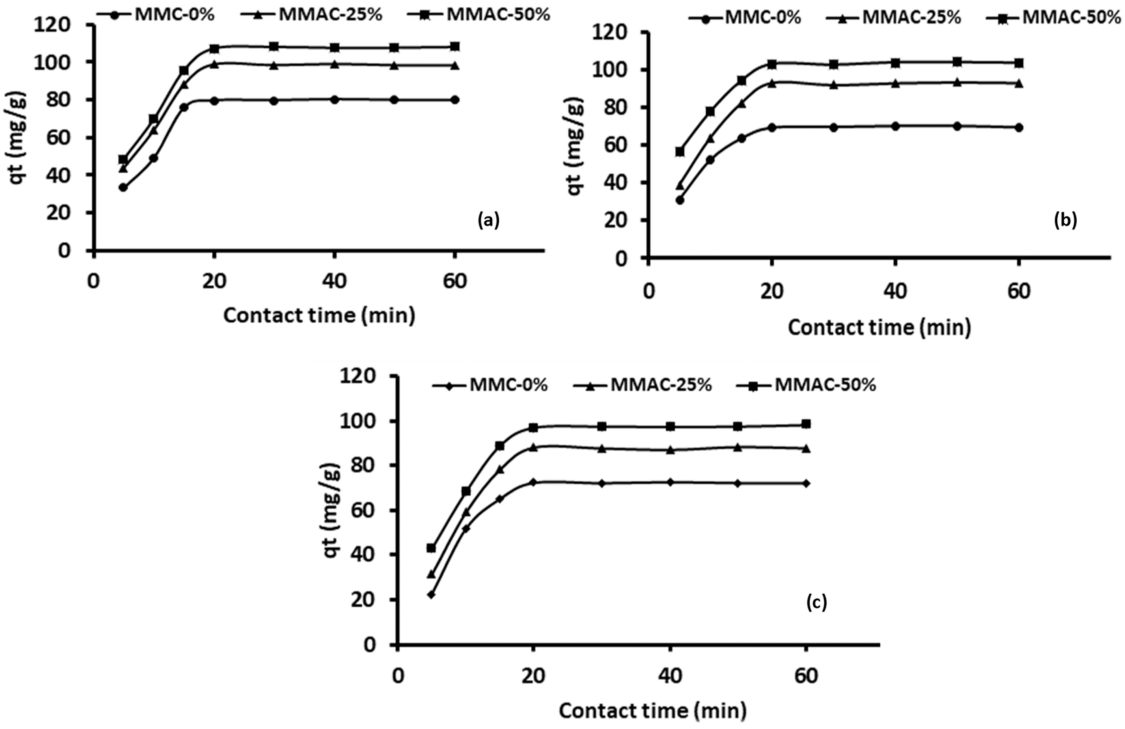


**Figure 7.** Effect of contact time on the adsorption of (a) ACT, (b) CAF, and (c) CBZ onto MMC-0%, MMAC-25%, and MMAC-50% adsorbents. Experimental conditions: initial concentration: 20 mg/L; mass of adsorbent: 56.2 mg; sample pH: 7; sample volume: 10 mL.

favorability of the analytes onto adsorbents.[64,67] According to previous studies, the adsorption process is favorable, irreversible, and linear if $0 < R_L < 1$, $R_L > 1$, $R_L = 0$, and $R_L = 1$, respectively.[68] In this study, the calculated $R_L$ value for MMC-0%, MMAC-25%, and MMAC-50% ranged from 0.083−0.15, 0.07−0.12, and 0.055−0.097, respectively, and these values were between 0 and 1, demonstrating that the adsorption of ACT, CAF, and CBZ onto these adsorbents was favorable. In the Freundlich isotherm, the parameter n indicates the adsorption intensity, and if $1 < n < 10$, this suggests that the sorption process is favorable. As seen in Table 2, the n values were greater than unity, indicating that the adsorption of ACT, CAF, and CBZ onto the adsorbents was favorable, and the active sites on the surface of the adsorbent were heterogeneous.[69] The $R^2$, RSE, and $\chi^2$ values for D-R isotherms (Table 2) showed that this model could also describe the adsorption of ACT, CAF, and CBZ onto the adsorbents. This model was then used to estimate the adsorption energy ($E_a$), which represents the nature of the sorption process. As seen in Table 2, the $E_a$ values were greater than 16 kJ/mol, suggesting that ACT, CAF, and CBZ adsorption onto MMC-0%, MMAC-25%, and MMAC-50% adsorbents chiefly occurred through chemisorption.[70,71]

*3.7.2. Three-Parameter Isotherm Models.* The adsorptive behavior of ACT, CAF, and CBZ on the adsorbents was further investigated using three-parameter isotherm models such as Redlich−Peterson and Sips. These isotherm models were chosen because they can be used in either homogeneous or heterogeneous systems.[72] Furthermore, Redlich−Peterson and Sips isotherm models were selected because they are hybrid adsorption mechanisms that could overcome the shortcomings of the Langmuir and Freundlich models.[73] The three-parameter isotherm and error function values derived from the nonlinear plots are presented in Table 3. The results show that both Sips and the Redlich−Peterson models gave high $R^2$ and low error values, indicating that both isotherms were the best fit for all of the adsorbents.

Additionally, the adsorption capacities estimated using the Sips model were closer to the experiment values, suggesting that depending on the initial concentrations of the analyte molecules, the adsorption of ACT, CAF, and CBZ happened on both monolayer sorption and heterogeneous surfaces of the adsorbents.[74,75] Furthermore, the surface heterogeneity values derived from the Sips model were close to 1 for the adsorbents, suggesting that the Langmuir equation predominantly describes the data. The heterogeneous surfaces of the mesoporous adsorbents might be from the ununiform distribution of hydroxyl and carboxylic groups, as seen by the bands 3410 and 1628 $cm^{-1}$ on the FTIR spectra.[76]

**3.8. Kinetics Studies.** The adsorption kinetics studies were conducted to understand the adsorption mechanism of ACT, CAF, and CBZ on the surfaces of magnetic mesoporous adsorbents. Figure 7 presents the results obtained from the three adsorbents. These revealed that a fast adsorption rate was achieved within the first 15 min, and then, the uptake of the analytes slowed to reach the adsorption equilibrium after 20 min. Furthermore, it was noted that the adoption capacities at time $t$ ($q_t$) of MMC-0%, MMAC-25%, and MMAC-50% adsorbents were significantly different. This was attributed to the difference in the physicochemical properties because the MMACs had higher $q_t$ values than MMC. This could be attributed to the increase in the oxygenated functional groups.[76] Furthermore, it was noted that the large specific surface area for MMAC-50 was found to be favorable for the simultaneous adsorption of ACT, CAF, and CBZ, thus increasing the removal efficiency of this adsorbent.

Four kinetic nonlinear models, including pseudo-first-order, pseudo-second-order, Elovich, and intraparticle diffusion, were used to explain the experimental data presented in Figure 7. Table 4 presents the kinetic parameters for pseudo-first-order,


https://doi.org/10.1021/acsomega.4c03426
ACS Omega 2024, 9, 34700−34718

Table 4. Nonlinear Adjusted Adsorption Kinetics and Parameters Investigated[a]

| models | parameters | MMC | | | MAC-25% | | | MAC-50% | | |
|---|---|---|---|---|---|---|---|---|---|---|
| | | ACT | CAF | CBZ | ACT | CAF | CBZ | ACT | CAF | CBZ |
| | $q_{exp}$ (mg/g) | 80.5 | 73.2 | 70.2 | 99.1 | 88.9 | 94.3 | 109 | 98.7 | 104 |
| PFO | $q_e$ (mg/g) | 72.1 | 65.6 | 63.9 | 82.7 | 71.9 | 81.8 | 93.2 | 86.8 | 88.1 |
| | $k_1$ (1/min) | 0.43 | 0.56 | 0.63 | 0.46 | 0.47 | 0.47 | 0.55 | 0.64 | 0.47 |
| | $R^2$ | 0.9635 | 0.9518 | 0.9781 | 0.9759 | 0.9838 | 0.9887 | 0.9837 | 0.9813 | 0.9871 |
| | RSE | 5.20 | 6.13 | 3.18 | 5.11 | 4.97 | 5.18 | 4.39 | 4.76 | 3.91 |
| | $\chi^2$ | 3.81 | 4.01 | 2.12 | 3.87 | 2.43 | 318 | 2.03 | 2.74 | 2.33 |
| PSO | $q_e$ (mg/g) | 82.0 | 74.5 | 72.7 | 101 | 90.3 | 94.9 | 110 | 99.6 | 103 |
| | $k_2$ (g/mg min) | 0.23 | 0.17 | 0.13 | 0.14 | 0.11 | 0.13 | 0.12 | 0.13 | 0.15 |
| | $R^2$ | 0.9918 | 0.9963 | 0.9982 | 0.9975 | 0.9979 | 0.9950 | 0.9981 | 0.9986 | 0.9972 |
| | RSE | 1.94 | 1.86 | 1.75 | 1.46 | 1.67 | 1.58 | 1.66 | 1.62 | 2.23 |
| | $\chi^2$ | 1.13 | 1.24 | 1.33 | 1.04 | 1.16 | 1.03 | 0.96 | 0.79 | 1.10 |
| Elovich | $\sigma$ (mg/g/min) | 35.4 | 25.5 | 47.6 | 48.3 | 32.3 | 44.9 | 52.9 | 55.4 | 52.8 |
| | $\beta$ (g/mg) | 0.054 | 0.055 | 0.077 | 0.045 | 0.047 | 0.048 | 0.041 | 0.047 | 0.057 |
| | $R^2$ | 0.9881 | 0.9873 | 0.9884 | 0.9793 | 0.9776 | 0.9876 | 0.9898 | 0.9889 | 0.9786 |
| | RSE | 2.18 | 2.34 | 2.01 | 2.30 | 2.52 | 3.57 | 2.75 | 2.92 | 3.77 |
| | $\chi^2$ | 1.82 | 1.77 | 1.48 | 1.83 | 1.45 | 1.32 | 1.81 | 1.73 | 1.69 |

[a] $q_e$ (mg/g): sorption capacity; $k_1$ (1/min): rate constant; $k_2$ (g/mg min): second-order constant; $\alpha$ (mg/g/min): initial rate constant; $\beta$: (g/mg) desorption constant.

pseudo-second-order, and Elovich models. The RSE, $\chi^2$, and $R^2$ values were used to select the models that best explain the experimental data. As seen, the experimental data were better described by the pseudo-second-order model followed by the Elovich kinetic model because they both had low RSE and $\chi^2$ values and high $R^2$. This trend was observed for all of the investigated adsorbents. In addition, the adsorption capacities obtained using the pseudo-second-order model were close to the experimental $q_e$ values, suggesting that the adsorption process might be dominated by chemisorption. Even though the pseudo-first-order model had high values of RSE and $\chi^2$ and lower $R^2$ values, the calculated adsorption capacity values using its nonlinear expression were closer to the experimental data values (Table 4), suggesting that there was a competition between physisorption and chemisorption.[77] The Elovich model was used to clarify the nature of ACT, CAF, and CBZ adsorption onto the adsorbents. As seen, the initial constant rate ($\alpha$) was found to be higher than the desorption coefficient ($\beta$) for all adsorbents. These results confirmed that the adsorption process was dominated by chemisorption,[78] thus agreeing with the isotherm results.

The kinetics data was fitted to the intraparticle diffusion model, and the adsorption of ACT, CAF, and CBZ onto the magnetic mesoporous adsorbents resulted in multilinear plots showing the adsorption process. The first stage was attributed to the external diffusion or mass transfer of analytes from the bulk solution to the external surface of the adsorbents. In contrast, the second step was ascribed to the diffusion of ACT, CAF, and CBZ molecules from the exterior surface to the internal pores of the magnetic mesoporous adsorbents.[79] The intraparticle diffusion kinetic model parameters are summarized in Table 5. Table 5 shows that boundary layer diffusion (C) values are not equal to zero, suggesting that the intraparticle diffusion is not the rate-limiting step. Therefore, it was concluded that the adsorption of ACT, CAF, and CBZ onto the surfaces of the adsorbents was concurrently governed by surface adsorption and intraparticle diffusion.

Furthermore, the intraparticle diffusion rate constant ($k_{ip1}$) for the first stage was higher than that for the second stage. This phenomenon was due to the availability of free adsorption sites and high concentrations of the analytes in the bulk solution. The ($k_{ip2}$) values for the second stage decrease significantly because of the continuing diffusion of analytes into the adsorbents' surface-active sites and inner pores.[79]

Table 5. Intraparticle Diffusion Kinetic Model Parameters[a]

| | analytes | parameter values | MMC-0% | MMAC-25% | MMAC-50% |
|---|---|---|---|---|---|
| step 1 | ACT | $k_{ip1}$ | 22.3 | 25.6 | 27.2 |
| | | $C_1$ | 16.9 | 14.3 | 13.2 |
| | | $R^2$ | 0.9524 | 0.9886 | 0.9884 |
| | CAF | $k_{ip}1$ | 22.6 | 25.8 | 24.9 |
| | | $C_1$ | 24.3 | 24.4 | 11.2 |
| | | $R^2$ | 0.9602 | 0.9878 | 0.9847 |
| | CBZ | $k_{ip1}$ | 17.2 | 24.5 | 21.0 |
| | | $C_1$ | 5.09 | 14.5 | 10.9 |
| | | $R^2$ | 0.9724 | 0.9940 | 0.9936 |
| step 2 | ACT | $k_{ip2}$ | 0.40 | 0.50 | 0.60 |
| | | $C_2$ | 77.3 | 98.1 | 103 |
| | | $R^2$ | 0.8121 | 0.8130 | 0.8926 |
| | CAF | $k_{ip2}$ | 0.38 | 0.29 | 0.33 |
| | | $C_2$ | 70.1 | 86.1 | 95.6 |
| | | $R^2$ | 0.9273 | 0.9173 | 0.8912 |
| | CBZ | $k_{ip2}$ | 0.31 | 0.71 | 0.68 |
| | | $C_2$ | 68.0 | 88.1 | 99.2 |
| | | $R^2$ | 0.8737 | 0.9241 | 0.7956 |

[a] C: intercept; $k_{ip}$: intraparticle diffusion rate constant.

**3.9. Adsorption Thermodynamics.** Thermodynamic studies were investigated to ascertain the dominant adsorption mechanisms (that is, physisorption or chemisorption). The adsorption process was carried out at different temperatures (25, 30, 35, and 40 °C). The thermodynamic parameters, such as enthalpy ($\Delta H°$), entropy ($\Delta S°$), and Gibbs energy ($\Delta G°$), were calculated according to the expressions reported in the literature.[80−83] The $\Delta H°$ and $\Delta S°$ values were estimated from regression equation parameters (slope and intercepts) of the van't Hoff plots. Table 6 presents the thermodynamic parameter values for ACT, CAF, and CBZ adsorption onto the surfaces of MMC-0%, MMAC-25%, and MMAC-50%



https://doi.org/10.1021/acsomega.4c03426
ACS Omega 2024, 9, 34700−34718

Table 6. Thermodynamics Parameter Values for ACT, CAF, and CBZ Adsorption onto MMC-0%, MMAC-25%, and MMAC-50% Adsorbents

| | | ACT | | | CAF | | | CBZ | | |
|---|---|---|---|---|---|---|---|---|---|---|
| parameters | $T$ (K) | MMC-0% | MMAC-25% | MMAC-50% | MMC-0% | MMAC-25% | MMAC-50% | MMC-0% | MMAC-25% | MMAC-50% |
| $\Delta G°$ (kJ/mol) | 298 | −6.67 | −7.88 | −6.23 | −5.89 | −5.78 | −5.68 | −6.12 | −5.48 | −5.27 |
| | 303 | −7.38 | −8.26 | −7.34 | −6.87 | −6.04 | −7.29 | −7.19 | −6.87 | −7.78 |
| | 308 | −8.93 | −9.49 | −8.93 | −8.75 | −7.93 | −8.33 | −9.25 | −7.98 | −9.06 |
| | 313 | −9.67 | −10.82 | −10.07 | −9.75 | −9.03 | −9.93 | −10.81 | −9.41 | −10.98 |
| $\Delta H$ (kJ/mol) | | −25.6 | −34.4 | −46.7 | −36.2 | −40.7 | −58.7 | −26.7 | −38.5 | −47.6 |
| $\Delta S°$(J/(mol·K)) | | −76.3 | −83.5 | −126 | −88.4 | −87.9 | −134 | −68.7 | −78.4 | −97.4 |

Table 7. Comparison of the Sorption Capacities for ACT, CAF, and CBZ on Various Activated Carbon Sorbents

| adsorbent | analyte | mass of adsorbent (mg) | sample volume (mL) | contact Time (hr) | Ph | adsorption capacity (mg/g) | refs |
|---|---|---|---|---|---|---|---|
| activated carbon (peanut shells) | CAF | 150 | 10 | 24 | 5 | 122 | 90 |
| activated carbon (coconut) | ACT | 80 | 10 | 24 | 7 | 5.96 | 89 |
| activated carbon (Babassu coconut biomass) | ACT | 10 | 20 | 24 | 3 | 128 | 86 |
| activated carbon (Argania Spinosa tree nutshells composites) | CBZ | 100 | 50 | 24 | 7 | 105.3 | 91 |
| biochar (coffee grounds) | CBZ | 50 | 20 | 24 | 7 | 19.89 | 92 |
| activated carbon (Cannabis sativum Hemp) | ACT | 20−120 | 25 | 0.5−8 | 3−11 | 16.18 | 94 |
| activated carbon (ceramic) | ACT | 15 | 15 | 24 | 7 | 159 | 87 |
| activated Carbon (cashew nutshell) | ACT | 12.5 | 25 | 24 | 7 | 146 | 88 |
| MMC-0% | ACT, CAF, CBZ | 56.2 | 10 | 0.5 | 7 | 81.7, 76.3, 73.5 | this study |
| MMAC-25% | ACT, CAF, CBZ | 56.2 | 10 | 0.5 | 7 | 102, 94.5, 98.7 | |
| MMAC-50% | ACT, CAF, CBZ | 56.2 | 10 | 0.5 | 7 | 112, 102, 106 | |

adsorbents. Table 6 shows that the $\Delta G°$ values were negative, suggesting that the simultaneous adsorption of the emerging contaminants onto the adsorbents was feasible, favorable, and spontaneous.[84] Moreover, the $\Delta G°$ values increase with increasing temperature, demonstrating that the efficiency of ACT, CAF, and CBZ adsorption onto the surface of magnetic mesoporous adsorbents was more favorable at higher temperatures.[84] The negative $\Delta H°$ reveals that the adsorption process was exothermic, and its values were higher than 20.9 kJ/mol, confirming that the chemisorption was dominant,[83] supporting prior observations from the isotherms and kinetics results. Furthermore, the negative $\Delta S°$ suggested a decrease in the randomness at the boundary of the solid/liquid phases during the adsorption process, and these results supported the affinity of magnetic mesoporous adsorbents toward the simultaneous adsorption of ACT, CAF, and CBZ.[85]

**3.10. Comparison Studies.** The adsorption methodology using activated carbon derived from PET plastics was compared with that of activated carbon derived from other waste materials documented in the literature to assess their analytical performance. The comparison was narrowed down to only the analytes (ACT, CAF, and CBZ) of interest. Table 7 summarizes the adsorbed emerging contaminant, some of the characteristic parameters of the activated carbon used as adsorbent, the pH, mass of adsorbent, contact time, and sample volume at which the adsorption process was analyzed, and the maximum adsorption capacity (mainly from the Langmuir's monolayer adsorption capacity but also) obtained from some of the studies previously reported in the literature. The adsorption capacities obtained in this study were high and comparable to the previous studies and followed the trend MMC > MMAC-25% > MMAC-50% for all three analytes. The obtained adsorption capacities for ACT ranged between 81.7−112 mg/g, which was lower compared to those reported elsewhere (Table 7).[86−88] This could be that Ferreira and co-workers used a lower pH, mass of adsorbent, high sample volume, and longer contact time, suggesting lower pH (Table 7) gave more ionic interactions and higher sample volume, which allowed more room for interactions for a longer time.[86] On the other hand, some researchers used similar pH conditions but higher sample volume and longer reaction time, which allowed for room and longer interactions between analytes and adsorbents.[87,88] However, a lower capacity obtained by Hamoudi and colleagues suggests that increased mass of adsorbent and longer reaction time did not have much influence on the adsorption capacities.[89] The adsorption capacities for CAF ranged between 76.3−102 mg/g, which were lower than those reported in the literature (Table 7).[90] This might be due to lower pH, which gives more ionic interactions, longer interactions, and more absorbency to remove the analyte. The capacities for CBZ (73.5−106 mg/g) were comparable to those reported by[91] and lower than the values reported by.[92] This suggests that CBZ was affected much by the higher adsorbent mass, sample volume, and longer reaction times. Moreover, adsorbent surface properties from various resources might also play a role in the adsorption capacities.[93]

**3.11. Regeneration and Reusability Studies.** The regeneration and reusability of the spent adsorbent are important parameters to be studied when investigating its practical application and the cost-effectiveness of the adsorption process for water treatment. Furthermore, it is important to examine the stability of an adsorbent because it is one of the critical uses in assessing the practical applicability


https://doi.org/10.1021/acsomega.4c03426
ACS Omega 2024, 9, 34700−34718

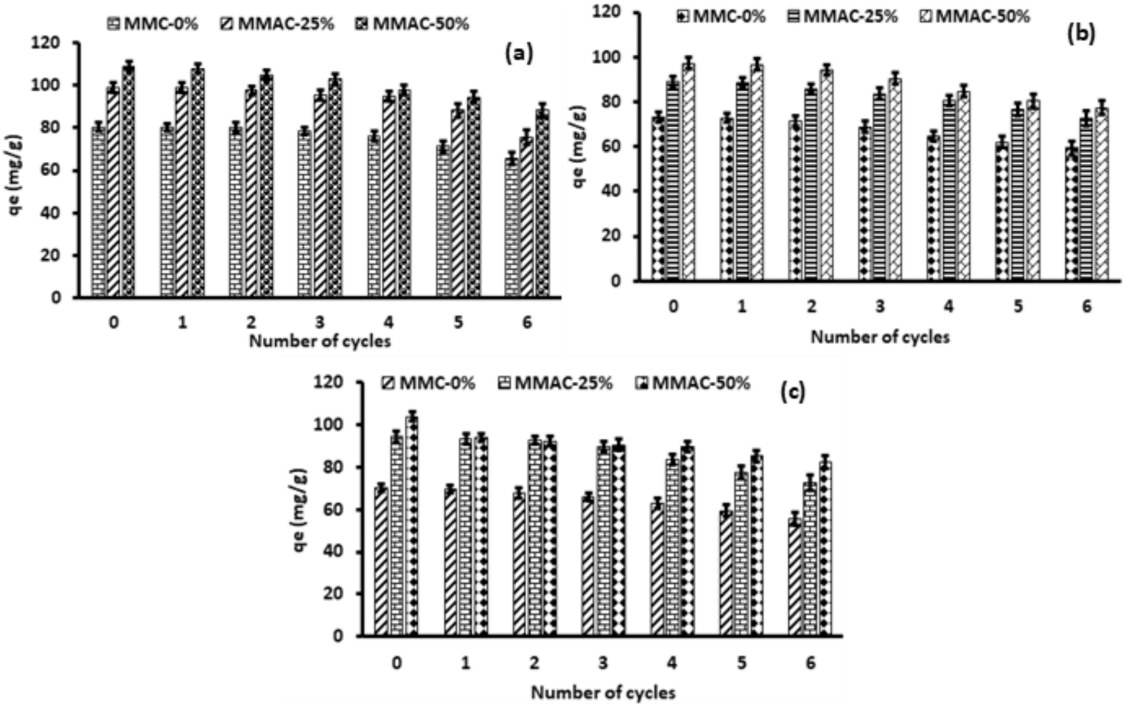


**Figure 8.** Regeneration and reusability studies of MMC-0%, MMAC-25%, and MMAC-50% adsorbents on the adsorption of (a) ACT, (b) CAF, and (c) CBZ. Experimental conditions: mass of absorbent: 56.2 mg; contact time: 30 min; temperature: 298 K; pH: 7.

**Table 8. Adsorption Performance of MMC-0%, MMAC-25%, and MMAC-50% Adsorbents for ACT, CAF, and CBZ Removal from Water Bodies ($n$ = 3)**

| | | %removal efficiency (mean ± %RSD) | | | | | |
|---|---|---|---|---|---|---|---|
| adsorbents | samples | ACT | | CAF | | CBZ | |
| | | 0.1 mg/L | 2.0 mg/L | 0.1 mg/L | 2.0 mg/L | 0.1 mg/L | 2.0 mg/L |
| MMC-0% | tap water | 99.5 ± 2.3 | 98.7 ± 2.5 | 99.1 ± 2.2 | 99.3 ± 2.1 | 99.6 ± 2.4 | 98.7 ± 2.6 |
| | surface water | 97.4 ± 2.3 | 95.5 ± 2.5 | 96.5 ± 2.3 | 98.1 ± 3.2 | 98.7 ± 2.4 | 96.7 ± 2.5 |
| | influent | 83.4 ± 2.3 | 76.7 ± 2.5 | 74 ± 2.2 | 68.8 ± 2.3 | 74.7 ± 2.3 | 72.7 ± 2.4 |
| | effluent | 88.2 ± 2.1 | 81.3 ± 2.4 | 78.1 ± 2.2 | 73.8 ± 2.5 | 79.3 ± 2.5 | 83.9 ± 2.2 |
| MMAC-25% | tap water | 100 ± 4 | 99.8 ± 3.2 | 99.8 ± 1.3 | 99.6 ± 1.6 | 100 ± 4 | 99.5 ± 2.4 |
| | surface water | 97.9 ± 2.2 | 96.1 ± 2.3 | 97.6 ± 2.5 | 98.5 ± 3.1 | 98.2 ± 2.5 | 97.7 ± 2.6 |
| | influent | 86.1 ± 2.5 | 81.5 ± 2.6 | 79.2 ± 2.8 | 72.2 ± 2.3 | 85.3 ± 2.3 | 84.1 ± 2.4 |
| | effluent | 90.2 ± 2.6 | 87.7 ± 2.7 | 85.6 ± 2.7 | 77.3 ± 2.5 | 90.1 ± 2.5 | 89.3 ± 2.2 |
| MMAC-50% | tap water | 100 ± 2 | 99.8 ± 2.5 | 100 ± 3 | 99.6 ± 3.1 | 100 ± 3 | 100 ± 2 |
| | surface water | 98.3 ± 2.5 | 97.5 ± 2.4 | 98.1 ± 2.2 | 98.6 ± 2.5 | 99.1 ± 2.1 | 98.2 ± 2.3 |
| | influent | 88.5 ± 2.7 | 87.3 ± 2.6 | 84.2 ± 2.3 | 76.8 ± 2.6 | 89.7 ± 2.2 | 88.7 ± 2.4 |
| | effluent | 92.7 ± 3.2 | 90.2 ± 2.3 | 89.4 ± 2.5 | 83.2 ± 2.7 | 93.3 ± 2.4 | 90.9 ± 2.5 |

and the possible secondary contamination caused by the spent adsorbent.[93] In this study, the reusability and regeneration of MMC-0%, MMAC-25%, and MMAC-50% adsorbents were assessed by conducting successive adsorption−desorption cycles repeated six times. As seen in Figure 8, the adsorption capacities of MMC-0%, MMAC-25%, and MMAC-50% adsorbents slightly decreased in the sixth adsorption−desorption cycle. The overall reduction of the adsorption capacities in the sixth adsorption−desorption cycle ranged from 18.2−23.6%. These results revealed that MMC-0%, MMAC-25%, and MMAC-50% adsorbents had good adsorption performance, and they were highly efficient and reusable. The leaching of iron from the magnetic adsorbents was evaluated to assess the stability of the sorbents. Iron was not detected in the solutions for all of the adsorption−desorption cycles when MMAC-25% and MMAC-50% adsorbents were used. However, for the MMC-0% adsorbent, traces of Fe ions (107−233 $\mu$g/L) were detected after the fifth adsorption−desorption cycle. The detected Fe concentrations were below the maximum allowable limits (300 $\mu$g/L). These results suggest that the prepared adsorbents could be safely used for the removal of emerging contaminants in water bodies with a very minimal possibility of causing secondary environmental pollution. Therefore, the prepared adsorbents displayed excellent stability, recoverability, separability, and reusability, thus making them promising adsorbents for industrial applications.

**3.12. Application of the Magnetic Mesoporous Adsorbents in Real Water Samples.** The applicability of the adsorption process using MMC-0%, MMAC-25%, and MMAC-50% adsorbents was evaluated for the adsorptive removal of ACT, CAF, and CBZ from different water samples,



https://doi.org/10.1021/acsomega.4c03426
ACS Omega 2024, 9, 34700−34718

such as domestic wastewater, surface water, and tap water. Tap water samples were used to compare the performance of the adsorbent to real complex samples. The physicochemical characteristics of the samples are presented in Table S1. The removal of the analytes was performed without adjustment of the pH of the water samples. This was done to maintain the environmental conditions of the samples. As seen in Table S1, the residual concentrations of ACT, CAF, and CBZ were detected in surface water, influent, and effluent wastewater samples. Table 8 presents the results obtained for the simultaneous removal of ACT, CAF, and CBZ in all water samples. As seen, the adsorption efficiency of the analytes in tap and surface water was greater than 95%. However, it decreased significantly, especially in wastewater effluents. The trend (MMC < MAC-25% < MAC-50%) was similar to all of the investigated real water samples. However, due to its high surface area, MMAC-50% displayed better removal efficiency compared to other adsorbents. The general decrease in the removal efficiency was attributed to the presence of high levels of coexisting substances in wastewater samples as compared to surface and tap water samples. These results suggest that some of the coexisting substances caused interferences in the adsorption of the analytes, thus resulting in the reduction of the adsorption efficiency of the target emerging contaminants.[93] The results obtained in this study also showed that the concentration of substances such as sulfates, COD, and turbidity significantly decreased after adsorption.

Furthermore, lower removal efficiency in wastewater samples was also attributed to the higher concentrations of ACT, CAF, and CBZ. Even though the performance of the adsorbents decreased in real wastewater samples, it is suspected that increasing the dosage of the adsorbents on a larger scale could lead to improved removal performance. Moreover, relatively high removal efficiencies ranging from 68.9 to 93.3% in wastewater samples indicated that the prepared magnetic mesoporous adsorbents are promising options for wastewater treatments.

## 4. CONCLUSIONS

Unique magnetic activated carbon adsorbents were successfully prepared from waste materials (PET plastics and AMD solutes) and applied for the adsorption of ACT, CAF, and CBZ from model solutions and real wastewater samples. The attractiveness of the surface properties of the prepared adsorbents was uncovered through the analysis of the physicochemical properties of the adsorbent by using techniques such as SEM, TEM, FTIR, XRD, BET, and $\zeta$ potential. The adsorbents were applied, and optimization of the parameters, such as pH and MA, was performed to adsorb the analytes from water. The optimum conditions (pH 6 and 56.2 mg of MA) obtained were satisfactory, considering the optimal performance of the adsorbents. The analytical performance of the adsorbents was examined in terms of equilibrium, kinetics, and thermodynamic studies. The nonlinear isotherm regression analysis data best fitted Langmuir and Freundlich models, suggesting that the adsorption process was monolayer adsorption on a heterogeneous adsorbent surface. The maximum adsorption capacity and Langmuir affinity constants for all of the analytes followed the trend: MMC-0% > MMAC-25% > MMAC-50%. The kinetic experimental data were better described by the pseudo-second-order model followed by the Elovich kinetic model due to low RSE and $\chi^2$ and high $R^2$ values. The adsorption capacities obtained using the pseudo-second-order model suggested that the adsorption process might be dominated by chemisorption, which the Elovich model also confirmed. The thermodynamics data revealed negative values of $\Delta G^\circ$, suggesting that the simultaneous adsorption was feasible, favorable, and spontaneous. The negative $\Delta H^\circ$ indicates that the adsorption process was exothermic, confirming that the chemisorption was dominant, and the negative $\Delta S^\circ$ suggested a decrease in the randomness at the boundary of the solid/liquid phases during the adsorption process. The magnetically activated carbon adsorbents were observed to be highly reusable, with satisfactory recovery for more than six cycles. Ultimately, the adsorbent was applied to real wastewater samples collected from a domestic WWTP. The potential applicability of the adsorbent was impressive for the extraction of selected analytes; this may be a solution for wastewater treatment systems that face the challenge of organic pollutants. The proposed method of waste conversion to functional adsorbent materials minimizes waste and removes other pollutants with high efficiency, which in turn will ensure a better circulation of waste, providing necessary key technologies for sustainable materials use.

## ■ ASSOCIATED CONTENT

### Supporting Information

The Supporting Information is available free of charge at https://pubs.acs.org/doi/10.1021/acsomega.4c03426.

Additional information, the instrumentation and sample preparation for characterization of the adsorbent, tables, including physicochemical properties of real samples and optimization of the experimental parameters, and figures, including FTIR, EDX, pore size distribution, selection of a suitable adsorbent, Pareto chart, $\zeta$ potential, and desirability function (PDF)

## ■ AUTHOR INFORMATION


### Corresponding Author

**Philiswa Nosizo Nomngongo** − *Department of Chemical Sciences, University of Johannesburg, Doornfontein 2028, South Africa; Department of Science and Innovation-National Research Foundation South African Research Chair Initiative (DSI-NRF SARChI) in Nanotechnology for Water and Department of Science and Innovation (DSI)/Mintek Nanotechnology Innovation Centre, University of Johannesburg, Doornfontein 2028, South Africa;* orcid.org/0000-0001-7615-0548; Email: pnnomngongo@uj.ac.za

### Authors

**Bongiwe Apatia Mvala** − *Department of Chemical Sciences, University of Johannesburg, Doornfontein 2028, South Africa; Department of Science and Innovation-National Research Foundation South African Research Chair Initiative (DSI-NRF SARChI) in Nanotechnology for Water and Department of Science and Innovation (DSI)/Mintek Nanotechnology Innovation Centre, University of Johannesburg, Doornfontein 2028, South Africa*

**Tshimangadzo S. Munonde** − *Department of Science and Innovation-National Research Foundation South African Research Chair Initiative (DSI-NRF SARChI) in Nanotechnology for Water, University of Johannesburg, Doornfontein 2028, South Africa; Institute for*




https://doi.org/10.1021/acsomega.4c03426
ACS Omega 2024, 9, 34700−34718

*Nanotechnology and Water Sustainability, College of Science, Engineering and Technology, University of South Africa, Roodepoort 1710, South Africa*

**Anele Mpupa** − *Department of Chemical Sciences, University of Johannesburg, Doornfontein 2028, South Africa; Department of Science and Innovation-National Research Foundation South African Research Chair Initiative (DSI-NRF SARChI) in Nanotechnology for Water, University of Johannesburg, Doornfontein 2028, South Africa*

**Mokae Fanuel Bambo** − *DSI/Mintek- Nanotechnology Innovation Centre, Advanced Materials, Mintek, Randburg 2125, South Africa*

**Kgabo Phillemon Matabola** − *DSI/Mintek- Nanotechnology Innovation Centre, Advanced Materials, Mintek, Randburg 2125, South Africa; Department of Water and Sanitation, University of Limpopo, Sovenga 0727, South Africa*

Complete contact information is available at: https://pubs.acs.org/10.1021/acsomega.4c03426

### Notes

The authors declare no competing financial interest.

## ■ ACKNOWLEDGMENTS

The authors gratefully acknowledge the Department of Science and Innovation-National Research Foundation South African Research Chair Initiative (DSI-NRF SARChI) funding instrument, grant no. 91230 and DSI/Mintek Nanotechnology Innovation Centre (NIC) for financial support. The authors are thankful to the Department of Chemical Sciences Faculty of Science at the University of Johannesburg.

## ■ REFERENCES

(1) Deng, W.; Li, N.; Zheng, H.; Lin, H. Occurrence and Risk Assessment of Antibiotics in River Water in Hong Kong. *Ecotoxicol. Environ. Saf.* **2016**, *125*, 121−127.

(2) Nazari, G.; Abolghasemi, H.; Esmaieli, M. Batch Adsorption of Cephalexin Antibiotic from Aqueous Solution by Walnut Shell-Based Activated Carbon. *J. Taiwan Inst. Chem. Eng.* **2016**, *58*, 357−365.

(3) Phong Vo, H. N.; Le, G. K.; Hong Nguyen, T. M.; Bui, X. T.; Nguyen, K. H.; Rene, E. R.; Vo, T. D. H.; Thanh Cao, N. D.; Mohan, R. Acetaminophen Micropollutant: Historical and Current Occurrences, Toxicity, Removal Strategies and Transformation Pathways in Different Environments. *Chemosphere* **2019**, *236*, No. 124391.

(4) Lofrano, G.; Libralato, G.; Meric, S.; Vaiano, V.; Sacco, O.; Venditto, V.; Guida, M.; Carotenuto, M. Occurrence and Potential Risks of Emerging Contaminants in Water. In *Visible Light Active Structured Photocatalysts for the Removal of Emerging Contaminants*; Elsevier, 2020; pp 1−25 DOI: 10.1016/B978-0-12-818334-2.00001-8.

(5) Pascale, R.; Bianco, G.; Coviello, D.; Cristina Lafiosca, M.; Masi, S.; Mancini, I. M.; Bufo, S. A.; Scrano, L.; Caniani, D. Validation of a Liquid Chromatography Coupled with Tandem Mass Spectrometry Method for the Determination of Drugs in Wastewater Using a Three-Phase Solvent System. *J. Sep. Sci.* **2020**, *43* (5), 886−895.

(6) Liu, Y.; Liu, X.; Dong, W.; Zhang, L.; Kong, Q.; Wang, W. Efficient Adsorption of Sulfamethazine onto Modified Activated Carbon: A Plausible Adsorption Mechanism. *Sci. Rep.* **2017**, *7* (1), No. 12437.

(7) Quesada, H. B.; Baptista, A. T. A.; Cusioli, L. F.; Seibert, D.; de Oliveira Bezerra, C.; Bergamasco, R. Surface Water Pollution by Pharmaceuticals and an Alternative of Removal by Low-Cost Adsorbents: A Review. *Chemosphere.* **2019**, *222*, 766−780.

(8) Carmona, E.; Andreu, V.; Picó, Y. Occurrence of Acidic Pharmaceuticals and Personal Care Products in Turia River Basin: From Waste to Drinking Water. *Sci. Total Environ.* **2014**, *484*, 53−63.

(9) Mokhtaryan, S.; Khodabakhshi, A.; Sadeghi, R.; Nourmoradi, H.; Shakeri, K.; Hemati, S.; Mohammadi-Moghadam, F. New Activated Carbon Derived from Gundelia Tournefortii Seeds for Effective Removal of Acetaminophen from Aqueous Solutions: Adsorption Performance. *Arabian J. Chem.* **2023**, *16* (11), No. 105253.

(10) Melliti, A.; Touihri, M.; Kofroňová, J.; Hannachi, C.; Sellaoui, L.; Bonilla-Petriciolet, A.; Vurm, R. Sustainable Removal of Caffeine and Acetaminophen from Water Using Biomass Waste-Derived Activated Carbon: Synthesis, Characterization, and Modelling. *Chemosphere* **2024**, *355*, No. 141787.

(11) Luo, Y.; Guo, W.; Ngo, H. H.; Nghiem, L. D.; Hai, F. I.; Zhang, J.; Liang, S.; Wang, X. C. A Review on the Occurrence of Micropollutants in the Aquatic Environment and Their Fate and Removal during Wastewater Treatment. *Sci. Total Environ.* **2014**, *473−474*, 619−641.

(12) Natarajan, R.; Anil Kumar, M.; Vaidyanathan, V. K. Synthesis and Characterization of Rhamnolipid Based Chitosan Magnetic Nanosorbents for the Removal of Acetaminophen from Aqueous Solution. *Chemosphere* **2022**, *288*, No. 132532.

(13) Amalraj Appavoo, I.; Hu, J.; Huang, Y.; Li, S. F. Y.; Ong, S. L. Response Surface Modeling of Carbamazepine (CBZ) Removal by Graphene-P25 Nanocomposites/UVA Process Using Central Composite Design. *Water Res.* **2014**, *57*, 270−279.

(14) Hu, C.; Li, J.; Ke, J.; Liang, J.; Liu, Q.; Wang, Q.; Huang, W. The Preparation and Removal Performance of Carbamazepine/Oxcarbazepine Double Template Magnetic Molecularly Imprinted Polymers. *Sep. Purif. Technol.* **2023**, *306*, No. 172309.

(15) Liu, W.; Chen, Y.; Wang, L.; Zhou, Y.; Chen, L.; Zhai, C.; Zhu, M. The Visible Optical Driving N-S Co-Doped La2Ti2O7 Activated Peroxydisulfate for Carbamazepine Removal: Mechanism and Performance. *Chem. Eng. J.* **2024**, *481*, No. 148632.

(16) Cruz del Álamo, A.; Puga, A.; Dias Soares, C. M.; Pariente, M. I.; Pazos, M.; Molina, R.; Sanromán, M. A.; Martínez, F.; Delerue-Matos, C. Novel 3D Electro-Fenton Reactor Based on a Catalytic Packed Bed Reactor of Perovskite/Carbon Microelectrodes for the Removal of Carbamazepine in Wastewater. *J. Environ. Chem. Eng.* **2024**, *12* (4), No. 113154.

(17) Bachmann, S. A. L.; Calvete, T.; Féris, L. A. Caffeine Removal from Aqueous Media by Adsorption: An Overview of Adsorbents Evolution and the Kinetic, Equilibrium and Thermodynamic Studies. *Sci. Total Environ.* **2021**, *767*, No. 144229.

(18) Aldeguer Esquerdo, A.; Varo Galvañ, P. J.; Sentana Gadea, I.; Prats Rico, D. Carbamazepine and Diclofenac Removal Double Treatment: Oxidation and Adsorption. *Int. J. Environ. Res. Public Health* **2021**, *18* (13), 7163.

(19) Escapa, C.; Coimbra, R. N.; Neuparth, T.; Torres, T.; Santos, M. M.; Otero, M. Acetaminophen Removal from Water by Microalgae and Effluent Toxicity Assessment by the Zebrafish Embryo Bioassay. *Water* **2019**, *11* (9), 1929.

(20) Simón-Herrero, C.; Naghdi, M.; Taheran, M.; Kaur Brar, S.; Romero, A.; Valverde, J. L.; Avalos Ramirez, A.; Sánchez-Silva, L. Immobilized Laccase on Polyimide Aerogels for Removal of Carbamazepine. *J. Hazard. Mater.* **2019**, *376*, 83−90.

(21) Vaithyanathan, V. K.; Ravi, S.; Leduc, R.; Vaidyanathan, V. K.; Cabana, H. Utilization of Biosolids for Glucose Oxidase Production: A Potential Bio-Fenton Reagent for Advanced Oxidation Process for Removal of Pharmaceutically Active Compounds. *J. Environ. Manage.* **2020**, *271*, No. 110995.

(22) Gil, A.; Taoufik, N.; García, A. M.; Korili, S. A. Comparative Removal of Emerging Contaminants from Aqueous Solution by Adsorption on an Activated Carbon. *Environ. Technol.* **2019**, *40* (23), 3017−3030.

(23) Wang, C.; Moore, N.; Bircher, K.; Andrews, S.; Hofmann, R. Full-Scale Comparison of UV/H2O2 and UV/Cl2 Advanced Oxidation: The Degradation of Micropollutant Surrogates and the Formation of Disinfection Byproducts. *Water Res.* **2019**, *161*, 448−458.

(24) Ma, R.; Zhang, S.; Wen, T.; Gu, P.; Li, L.; Zhao, G.; Niu, F.; Huang, Q.; Tang, Z.; Wang, X. A Critical Review on Visible-Light-

Response CeO2-Based Photocatalysts with Enhanced Photooxidation of Organic Pollutants. *Catal. Today* **2019**, *335*, 20−30.
(25) Nivala, J.; Kahl, S.; Boog, J.; van Afferden, M.; Reemtsma, T.; Müller, R. A. Dynamics of Emerging Organic Contaminant Removal in Conventional and Intensified Subsurface Flow Treatment Wetlands. *Sci. Total Environ.* **2019**, *649*, 1144−1156.
(26) Díaz-Garduño, B.; Pintado-Herrera, M. G.; Biel-Maeso, M.; Rueda-Márquez, J. J.; Lara-Martín, P. A.; Perales, J. A.; Manzano, M. A.; Garrido-Pérez, C.; Martín-Díaz, M. L. Environmental Risk Assessment of Effluents as a Whole Emerging Contaminant: Efficiency of Alternative Tertiary Treatments for Wastewater Depuration. *Water Res.* **2017**, *119*, 136−149.
(27) Yao, M.; Duan, L.; Wei, J.; Qian, F.; Hermanowicz, S. W. Carbamazepine Removal from Wastewater and the Degradation Mechanism in a Submerged Forward Osmotic Membrane Bioreactor. *Bioresour. Technol.* **2020**, *314*, No. 123732.
(28) Mahlangu, T. O.; Hoek, E. M. V.; Mamba, B. B.; Verliefde, A. R. D. Influence of Organic, Colloidal and Combined Fouling on NF Rejection of NaCl and Carbamazepine: Role of Solute-Foulant-Membrane Interactions and Cake-Enhanced Concentration Polarisation. *J. Membr. Sci.* **2014**, *471*, 35−46.
(29) He, Q.; Liang, J. J.; Chen, L. X.; Chen, S. L.; Zheng, H. L.; Liu, H. X.; Zhang, H. J. Removal of the Environmental Pollutant Carbamazepine Using Molecular Imprinted Adsorbents: Molecular Simulation, Adsorption Properties, and Mechanisms. *Water Res.* **2020**, *168*, No. 115164.
(30) Nielsen, L.; Bandosz, T. J. Analysis of the Competitive Adsorption of Pharmaceuticals on Waste Derived Materials. *Chem. Eng. J.* **2016**, *287*, 139−147.
(31) Rovani, S.; Censi, M. T.; Pedrotti, S. L.; Lima, É. C.; Cataluña, R.; Fernandes, A. N. Development of a New Adsorbent from Agro-Industrial Waste and Its Potential Use in Endocrine Disruptor Compound Removal. *J. Hazard. Mater.* **2014**, *271*, 311−320.
(32) Cunha, M. R.; Lima, E. C.; Cimirro, N. F. G. M.; Thue, P. S.; Dias, S. L. P.; Gelesky, M. A.; Dotto, G. L.; dos Reis, G. S.; Pavan, F. A. Conversion of Eragrostis Plana Nees Leaves to Activated Carbon by Microwave-Assisted Pyrolysis for the Removal of Organic Emerging Contaminants from Aqueous Solutions. *Environ. Sci. Pollut. Res.* **2018**, *25* (23), 23315−23327.
(33) Lima, D. R.; Hosseini-Bandegharaei, A.; Thue, P. S.; Lima, E. C.; de Albuquerque, Y. R. T.; dos Reis, G. S.; Umpierres, C. S.; Dias, S. L. P.; Tran, H. N. Efficient Acetaminophen Removal from Water and Hospital Effluents Treatment by Activated Carbons Derived from Brazil Nutshells. *Colloids Surf., A* **2019**, *583*, No. 123966.
(34) Chan, K.; Zinchenko, A. Design and Synthesis of Functional Materials by Chemical Recycling of Waste Polyethylene Terephthalate (PET) Plastic: Opportunities and Challenges. *J. Cleaner Prod.* **2023**, *433*, No. 139828.
(35) Adeniran, A. A.; Shakantu, W. The Health and Environmental Impact of Plastic Waste Disposal in South African Townships: A Review. *Int. J. Environ. Res. Public Health* **2022**, *19* (2), 779.
(36) Hogsden, K. L.; Harding, J. S. Consequences of Acid Mine Drainage for the Structure and Function of Benthic Stream Communities: A Review. *Freshwater Sci.* **2012**, *31* (1), 108−120.
(37) Pandey, P.; Dhiman, M.; Kansal, A.; Subudhi, S. P. Plastic Waste Management for Sustainable Environment: Techniques and Approaches. *Waste Disposal Sustainable Energy* **2023**, *5*, 205−222.
(38) Singh, E.; Kumar, A.; Mishra, R.; You, S.; Singh, L.; Kumar, S.; Kumar, R. Pyrolysis of Waste Biomass and Plastics for Production of Biochar and Its Use for Removal of Heavy Metals from Aqueous Solution. *Bioresour. Technol.* **2021**, *320*, No. 124278.
(39) Blanchard, R.; Mekonnen, T. H. Synchronous Pyrolysis and Activation of Poly (Ethylene Terephthalate) for the Generation of Activated Carbon for Dye Contaminated Wastewater Treatment. *J. Environ. Chem. Eng.* **2022**, *10* (6), No. 108810.
(40) Wei, X.; Viadero, R. C. Synthesis of Magnetite Nanoparticles with Ferric Iron Recovered from Acid Mine Drainage: Implications for Environmental Engineering. *Colloids Surf., A* **2007**, *294*, 280−286.
(41) Chan, K.; Zinchenko, A. Functional Upcycling of Waste PET Plastic to the Hybrid Magnetic Microparticles Adsorbent for Cesium Removal. *Chemosphere* **2024**, *354*, No. 141725.
(42) Dyosiba, X.; Ren, J.; Musyoka, N. M.; Langmi, H. W.; Mathe, M.; Onyango, M. S. Preparation of Value-Added Metal-Organic Frameworks (MOFs) Using Waste PET Bottles as Source of Acid Linker. *Sustainable Mater. Technol.* **2016**, *10*, 10−13.
(43) Akinwekomi, V.; Maree, J. P.; Masindi, V.; Zvinowanda, C.; Osman, M. S.; Foteinis, S.; Mpenyana-Monyatsi, L.; Chatzisymeon, E. Beneficiation of Acid Mine Drainage (AMD): A Viable Option for the Synthesis of Goethite, Hematite, Magnetite, and Gypsum − Gearing towards a Circular Economy Concept. *Miner. Eng.* **2020**, *148*, No. 106204.
(44) Liu, Y.; Meng, H.; Konst, S.; Sarmiento, R.; Rajachar, R.; Lee, B. P. Injectable Dopamine-Modified Poly(Ethylene Glycol) Nanocomposite Hydrogel with Enhanced Adhesive Property and Bioactivity. *ACS Appl. Mater. Interfaces* **2014**, *6* (19), 16982−16992.
(45) M Awwad, A.; M Salem, N. A Green and Facile Approach for Synthesis of Magnetite Nanoparticles. *Nanosci. Nanotechnol.* **2012**, *2* (6), 208−213.
(46) Siddiqui, M. T. H.; Nizamuddin, S.; Baloch, H. A.; Mubarak, N. M.; Dumbre, D. K.; Inamuddin; Asiri, A. M.; Bhutto, A. W.; Srinivasan, M.; Griffin, G. J. Synthesis of Magnetic Carbon Nanocomposites by Hydrothermal Carbonization and Pyrolysis. *Environ. Chem. Lett.* **2018**, *16*, 821−844.
(47) Yuan, Z. Y.; Su, B. L. Surfactant-Assisted Nanoparticle Assembly of Mesoporous $\beta$-FeOOH (Akaganeite). *Chem. Phys. Lett.* **2003**, *381*, 710−714.
(48) de Oliveira Carvalho, C.; Costa Rodrigues, D. L.; Lima, É. C.; Santanna Umpierres, C.; Caicedo Chaguezac, D. F.; Machado Machado, F. Kinetic, Equilibrium, and Thermodynamic Studies on the Adsorption of Ciprofloxacin by Activated Carbon Produced from Jerivá (Syagrus Romanzoffiana). *Environ. Sci. Pollut. Res.* **2019**, *26* (5), 4690−4702.
(49) Jain, A.; Balasubramanian, R.; Srinivasan, M. P. Production of High Surface Area Mesoporous Activated Carbons from Waste Biomass Using Hydrogen Peroxide-Mediated Hydrothermal Treatment for Adsorption Applications. *Chem. Eng. J.* **2015**, *273*, 622−629.
(50) Mészáros, P.; Kovács, S.; Kulcsár, G.; Páskuj, M.; Almási, A. Investigation of Intestinal Absorption and Excretion of Paracetamol in Streptozotocin-Induced Hyperglycemia. *Int. J. Mol. Sci.* **2022**, *23* (19), No. 11913.
(51) Fakioğlu, M.; Kalpaklı, Y. Mechanism and Behavior of Caffeine Sorption: Affecting Factors. *RSC Adv.* **2022**, *12*, 26504−26513.
(52) Alvarado, A. T.; Paredes, G.; García, G.; Morales, A.; Muñoz, A. M.; Saravia, M.; Losno, R.; Bendezú, M. R.; Chávez, H.; García, J. A.; Pineda, M.; Sullón-Dextre, L.; et al. Serum Monitoring of Carbamazepine in Patients with Epilepsy and Clinical Implications. *Pharmacia* **2022**, *69* (2), 401−406.
(53) Xing, X.; Zhang, Y.; Zhou, G.; Zhang, Y.; Yue, J.; Wang, X.; Yang, Z.; Chen, J.; Wang, Q.; Zhang, J. Mechanisms of Polystyrene Nanoplastics Adsorption onto Activated Carbon Modified by ZnCl2. *Sci. Total Environ.* **2023**, *876*, No. 162763.
(54) Ayawei, N.; Ebelegi, A. N.; Wankasi, D. Modelling and Interpretation of Adsorption Isotherms. *J. Chem.* **2017**, *2017*, 1−11.
(55) El Din Mahmoud, A.; Fawzy, M. Bio-Based Methods for Wastewater Treatment: Green Sorbents. *Phytoremediation* **2016**, *3*, 209−238.
(56) Zhang, F.; Chen, X.; Wu, F.; Ji, Y. High Adsorption Capability and Selectivity of ZnO Nanoparticles for Dye Removal. *Colloids Surf., A* **2016**, *509*, 474−483.
(57) Okpara, O. G.; Ogbeide, O. M.; Ike, O. C.; Menechukwu, K. C.; Ejike, E. C. Optimum Isotherm by Linear and Nonlinear Regression Methods for Lead (II) Ions Adsorption from Aqueous Solutions Using Synthesized Coconut Shell−Activated Carbon (SCSAC). *Toxin Rev.* **2021**, *40* (4), 901−914.
(58) Batool, F.; Akbar, J.; Iqbal, S.; Noreen, S.; Bukhari, S. N. A. Study of Isothermal, Kinetic, and Thermodynamic Parameters for Adsorption of Cadmium: An Overview of Linear and Nonlinear


https://doi.org/10.1021/acsomega.4c03426
*ACS Omega* 2024, 9, 34700−34718

Approach and Error Analysis. *Bioinorg. Chem. Appl.* **2018**, *2018*, No. 463724.
(59) Hamzaoui, M.; Bestani, B.; B, N. The Use of Linear and Nonlinear Methods for Adsorption Isotherm Optimization of Basic Green 4-Dye onto Sawdust-Based Activated Carbon. *J. Mater. Environ. Sci.* **2018**, *9* (4), 1110−1118.
(60) Deb, H.; Hasan, K.; Islam, M. Z.; Kai, L.; Yang, S.; Zhang, Y.; Yao, J. The Statistical Error Optimization of Dye Sorption Equilibria for the Precise Prediction of Adsorption Isotherms on Activated Graphene. *Appl. Sci.* **2023**, *13* (14), 8106.
(61) Watwe, V.; Bandal, G.; Kulkarni, P. Source-Normalized Error Analysis Method for Accurate Prediction of Adsorption Isotherm: Application to Cu(II) Adsorption on PVA-Blended Alginate Beads. *J. Iran. Chem. Soc.* **2023**, *20* (4), 949−959.
(62) Shikuku, V. O.; Jemutai-Kimosop, S. Efficient Removal of Sulfamethoxazole onto Sugarcane Bagasse-Derived Biochar: Two and Three-Parameter Isotherms, Kinetics and Thermodynamics. *South African J. Chem.* **2020**, *73* (1), 111−119.
(63) López-Luna, J.; Ramírez-Montes, L. E.; Martinez-Vargas, S.; Martínez, A. I.; Mijangos-Ricardez, O. F.; González-Chávez, M. del C. A.; Carrillo-González, R.; Solís-Domínguez, F. A.; Cuevas-Díaz, M. del C.; Vázquez-Hipólito, V. Linear and Nonlinear Kinetic and Isotherm Adsorption Models for Arsenic Removal by Manganese Ferrite Nanoparticles. *SN Appl. Sci.* **2019**, *1* (8), No. 27.
(64) Wakejo, W. K.; Meshesha, B. T.; Kang, J. W.; Demesa, A. G. Bamboo Sawdust-Derived High Surface Area Activated Carbon for Remarkable Removal of Paracetamol from Aqueous Solution: Sorption Kinetics, Isotherm, Thermodynamics, and Regeneration Studies. *Water Pract. Technol.* **2023**, *18* (6), 1366−1388.
(65) Li, J.; Yu, G.; Pan, L.; Li, C.; You, F.; Xie, S.; Wang, Y.; Ma, J.; Shang, X. Study of Ciprofloxacin Removal by Biochar Obtained from Used Tea Leaves. *J. Environ. Sci.* **2018**, *73*, 20−30.
(66) Fan, S.; Tang, J.; Wang, Y.; Li, H.; Zhang, H.; Tang, J.; Wang, Z.; Li, X. Biochar Prepared from Co-Pyrolysis of Municipal Sewage Sludge and Tea Waste for the Adsorption of Methylene Blue from Aqueous Solutions: Kinetics, Isotherm, Thermodynamic and Mechanism. *J. Mol. Liq.* **2016**, *220*, 432−441.
(67) El-Azazy, M.; El-Shafie, A. S.; Morsy, H. Biochar of Spent Coffee Grounds as per Se and Impregnated with Tio2: Promising Waste-Derived Adsorbents for Balofloxacin. *Molecules* **2021**, *26* (8), 2295.
(68) Liu, L.; Lin, Y.; Liu, Y.; Zhu, H.; He, Q. Removal of Methylene Blue from Aqueous Solutions by Sewage Sludge Based Granular Activated Carbon: Adsorption Equilibrium, Kinetics, and Thermodynamics. *J. Chem. Eng. Data* **2013**, *58* (8), 2248−2253.
(69) Alver, E.; Metin, A. ü. Anionic Dye Removal from Aqueous Solutions Using Modified Zeolite: Adsorption Kinetics and Isotherm Studies. *Chem. Eng. J.* **2012**, *200*−*202*, 59−67.
(70) Kamaraj, R.; Pandiarajan, A.; Jayakiruba, S.; Naushad, M.; Vasudevan, S. Kinetics, Thermodynamics and Isotherm Modeling for Removal of Nitrate from Liquids by Facile One-Pot Electrosynthesized Nano Zinc Hydroxide. *J. Mol. Liq.* **2016**, *215*, 204−211.
(71) Chen, S.; Qin, C.; Wang, T.; Chen, F.; Li, X.; Hou, H.; Zhou, M. Study on the Adsorption of Dyestuffs with Different Properties by Sludge-Rice Husk Biochar: Adsorption Capacity, Isotherm, Kinetic, Thermodynamics and Mechanism. *J. Mol. Liq.* **2019**, *285*, 62−74.
(72) Kalam, S.; Abu-Khamsin, S. A.; Kamal, M. S.; Patil, S. Surfactant Adsorption Isotherms: A Review. *ACS Omega* **2021**, *6*, 32342−32348.
(73) Duman, G. Preparation of Novel Porous Carbon from Hydrothermal Pretreated Textile Wastes: Effects of Textile Type and Activation Agent on Structural and Adsorptive Properties. *J. Water Process Eng.* **2021**, *43*, No. 102286.
(74) Daneshvar, E.; Vazirzadeh, A.; Niazi, A.; Kousha, M.; Naushad, M.; Bhatnagar, A. Desorption of Methylene Blue Dye from Brown Macroalga: Effects of Operating Parameters, Isotherm Study and Kinetic Modeling. *J. Cleaner Prod.* **2017**, *152*, 443−453.
(75) Guediri, A.; Bouguettoucha, A.; Chebli, D.; Chafai, N.; Amrane, A. Molecular Dynamic Simulation and DFT Computational Studies on the Adsorption Performances of Methylene Blue in Aqueous Solutions by Orange Peel-Modified Phosphoric Acid. *J. Mol. Struct.* **2020**, *1202*, No. 127290.
(76) Yang, X.; Wan, Y.; Zheng, Y.; He, F.; Yu, Z.; Huang, J.; Wang, H.; Ok, Y. S.; Jiang, Y.; Gao, B. Surface Functional Groups of Carbon-Based Adsorbents and Their Roles in the Removal of Heavy Metals from Aqueous Solutions: A Critical Review. *Chem. Eng. J.* **2019**, *366*, 608−621.
(77) Agbor Tabi, G.; Ngouateu Rene Blaise, L.; Daouda, K.; Naphtali Odogu, A.; Aime Victoire, A.; Nsami Julius, N.; Joseph Mbadcam, K. Non-Linear Modelling of the Adsorption of Indigo Carmine Dye from Wastewater onto Characterized Activated Carbon/Volcanic Ash Composite. *Arabian J. Chem.* **2022**, *15* (1), No. 103515.
(78) Basha, I. K.; Abd El-Monaem, E. M.; Khalifa, R. E.; Omer, A. M.; Eltaweil, A. S. Sulfonated Graphene Oxide Impregnated Cellulose Acetate Floated Beads for Adsorption of Methylene Blue Dye: Optimization Using Response Surface Methodology. *Sci. Rep.* **2022**, *12* (1), No. 9339.
(79) Gabr, S. S.; Mubarak, M. F.; Keshawy, M.; El Sayed, I. E. T.; Abdel Moghny, T. Linear and Nonlinear Regression Analysis of Phenol and P-Nitrophenol Adsorption on a Hybrid Nanocarbon of ACTF: Kinetics, Isotherm, and Thermodynamic Modeling. *Appl. Water Sci.* **2023**, *13* (12), 230.
(80) Mashile, G. P.; Mpupa, A.; Nqombolo, A.; Dimpe, K. M.; Nomngongo, P. N. Recyclable Magnetic Waste Tyre Activated Carbon-Chitosan Composite as an Effective Adsorbent Rapid and Simultaneous Removal of Methylparaben and Propylparaben from Aqueous Solution and Wastewater. *J. Water Process Eng.* **2020**, *33*, No. 101011.
(81) Nagy, B.; Mânzatu, C.; Măicăneanu, A.; Indolean, C.; Barbu-Tudoran, L.; Majdik, C. Linear and Nonlinear Regression Analysis for Heavy Metals Removal Using Agaricus Bisporus Macrofungus. *Arabian J. Chem.* **2017**, *10*, No. 101011.
(82) Aazza, M.; Ahlafi, H.; Moussout, H.; Maghat, H. Adsorption of Metha-Nitrophenol onto Alumina and HDTMA Modified Alumina: Kinetic, Isotherm and Mechanism Investigations. *J. Mol. Liq.* **2018**, *268*, 587−597.
(83) Liu, Y.; Xiong, Y.; Xu, P.; Pang, Y.; Du, C. Enhancement of Pb (II) Adsorption by Boron Doped Ordered Mesoporous Carbon: Isotherm and Kinetics Modeling. *Sci. Total Environ.* **2020**, *708*, No. 134918.
(84) Shahinpour, A.; Tanhaei, B.; Ayati, A.; Beiki, H.; Sillanpää, M. Binary Dyes Adsorption onto Novel Designed Magnetic Clay-Biopolymer Hydrogel Involves Characterization and Adsorption Performance: Kinetic, Equilibrium, Thermodynamic, and Adsorption Mechanism. *J. Mol. Liq.* **2022**, *366*, No. 120303.
(85) Singh, M.; Ahsan, M.; Pandey, V.; Singh, A.; Mishra, D.; Tiwari, N.; Singh, P.; Karak, T.; Khare, P. Comparative Assessment for Removal of Anionic Dye from Water by Different Waste-Derived Biochar Vis a Vis Reusability of Generated Sludge. *Biochar* **2022**, *4* (1), No. 13.
(86) Ferreira, R. C.; de Araújo, T. P.; Dias, D.; Bernardo, M.; Lapa, N.; Fonseca, I. M.; de Barros, M. A. S. D. Removal of Paracetamol and Cu2+ from Water by Using Porous Carbons Derived from Agrowastes. *Processes* **2023**, *11* (7), 2146.
(87) Bursztyn Fuentes, A. L.; Benito, D. E.; Montes, M. L.; Scian, A. N.; Lombardi, M. B. Paracetamol and Ibuprofen Removal from Aqueous Phase Using a Ceramic-Derived Activated Carbon. *Arabian J. Chem.* **2023**, *48* (1), 525−537.
(88) Geczo, A.; Giannakoudakis, D. A.; Triantafyllidis, K.; Elshaer, M. R.; Rodríguez-Aguado, E.; Bashkova, S. Mechanistic Insights into Acetaminophen Removal on Cashew Nut Shell Biomass-Derived Activated Carbons. *Environ. Sci. Pollut. Res.* **2021**, *28* (42), 58969−58982.
(89) Ait Hamoudi, S.; Brahimi, M.; Boucha, M.; Hamdi, B.; Arrar, J. Removal of Paracetamol from Aqueous Solution by Containment Composites. *Open Chem.* **2021**, *19* (1), 49−59.


https://doi.org/10.1021/acsomega.4c03426
*ACS Omega* 2024, 9, 34700−34718

(90) Onaga Medina, F. M.; Aguiar, M. B.; Parolo, M. E.; Avena, M. J. Insights of Competitive Adsorption on Activated Carbon of Binary Caffeine and Diclofenac Solutions. *J. Environ. Manage.* **2021**, *278*, No. 111523.
(91) El Mouchtari, E. M.; Daou, C.; Rafqah, S.; Najjar, F.; Anane, H.; Piram, A.; Hamade, A.; Briche, S.; Wong-Wah-Chung, P. TiO2 and Activated Carbon of Argania Spinosa Tree Nutshells Composites for the Adsorption Photocatalysis Removal of Pharmaceuticals from Aqueous Solution. *J. Photochem. Photobiol. A Chem.* **2020**, *388*, No. 112183.
(92) Shin, J.; Lee, Y. G.; Lee, S. H.; Kim, S.; Ochir, D.; Park, Y.; Kim, J.; Chon, K. Single and Competitive Adsorptions of Micropollutants Using Pristine and Alkali-Modified Biochars from Spent Coffee Grounds. *J. Hazard. Mater.* **2020**, *400*, No. 123102.
(93) De Gisi, S.; Lofrano, G.; Grassi, M.; Notarnicola, M. Characteristics and Adsorption Capacities of Low-Cost Sorbents for Wastewater Treatment: A Review. *Sustainable Mater. Technol.* **2016**, *9*, 10−40.
(94) Sajid, M.; Bari, S.; Saif Ur Rehman, M.; Ashfaq, M.; Guoliang, Y.; Mustafa, G. Adsorption Characteristics of Paracetamol Removal onto Activated Carbon Prepared from Cannabis Sativum Hemp. *Alexandria Eng. J.* **2022**, *61* (9), 7203−7212.


https://doi.org/10.1021/acsomega.4c03426
*ACS Omega* 2024, 9, 34700−34718